Radiation Resilience: Taming the Cosmic Storm with Brain-Inspired Computers

An Exploratory Research to Characterize and Mitigate Radiation Effects in Mixed-Signal Neuromorphic Processors for Space Applications

J.F.R.W. Kievits

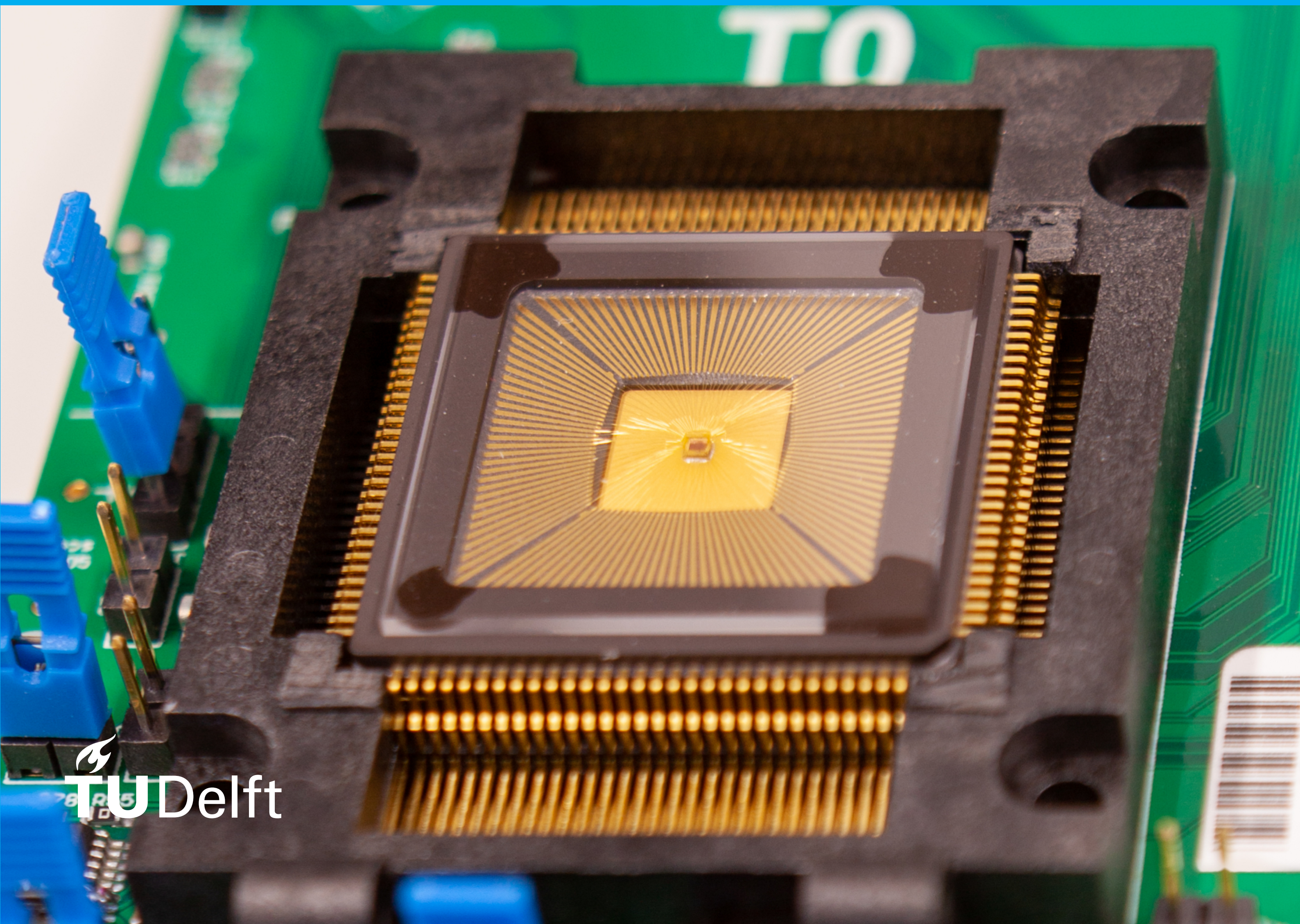

Radiation Resilience: Taming the Cosmic Storm with Brain-Inspired Computers

An Exploratory Research to Characterize and Mitigate Radiation Effects in Mixed-Signal Neuromorphic Processors for Space Applications

by

J.F.R.W. Kievits

in partial fulfillment of the requirements for the degree of

Master of Science
in Aerospace, Aeronautical and Astronautical Engineering

at the Delft University of Technology,
to be defended publicly on Thursday, June 22, 2023, at 14:00.

Student number:	4448693	
Project duration:	July 1, 2022 – June 22, 2023	
Thesis committee:		
	dr. P. A. Bogdan,	Innatera Nanosystems B.V.
	dr. A. Cervone,	TU Delft
	dr. A. Menicucci,	TU Delft
	dr. ir. T. G. R. M. van Leuken,	TU Delft / Innatera Nanosystems B.V.

Preface

Firstly, I would like to thank my supervisor from the TU Delft, Alessandra Menicucci, for her guiding advice during this entire project. Especially during the first phases of the research, you have helped me distinguish my (overly-optimistic) ambitions from achievable scientific goals. Your expert opinion on everything space-related has been an incredibly useful input for me to find relevant research topics and material. Without it, this research project could have easily lasted several years...

I'd also like to thank Petrut Bogdan from Innatera, my teacher and sparring partner for all topics related to spiking neural networks and neuromorphic computing. You mentioned at the beginning of the project that this would be an invaluable learning experience for me. It is only thanks to your sharp scientific and professional guidance that this was indeed the case.

Another person I owe thanks to is Wouter van Burik from HollandPTC. I am not sure if you enjoyed our evenings at the facility as much as I did, but your professionalism and enthusiasm certainly improved what could have been a monotonous and lengthy experience, dominated by repetitive phrases like "beam on" and "beam off"...

For my housemates, family, and friends, I am truly grateful for your listening ear and positive attitude whenever I would bring up my thesis. Although I will continue researching this awesome topic, I will try to burden you less heavily and stop ruining the fun dinner conversations...

J.F.R.W. Kievits
June 20, 2023

Contents

List of Figures

List of Tables

Glossary

AI	Artificial Intelligence
ANN	Artificial Neural Network
CME	Coronal Mass Ejection
COTS	Commercial-Off-The-Shelf
CPU	Central Processing Unit
DAC	Digital-to-Analog Converter
DD	Displacement Damage
DNN	Deep Neural Network
DUT	Device Under Test
EDAC	Error Detection and Correction
ECC	Error Correcting Code
EO	Earth Observation
EPSP	Excitatory Postsynaptic Potential
ERB	Earth’s Radiation Belt
ESA	European Space Agency
ESD	Electrostatic Discharge
FPGA	Field-Programmable Gate Array
GCR	Galactic Cosmic Rays
GUI	Graphical User Interface
HH	Hodgkin-Huxley
IC	Integrated Circuit
IPSP	Inhibitory Postsynaptic Potential
ISI	Inter-Spike Interval
LEO	Low Earth Orbit
LIF	Leaky-Integrate-and-Fire
MBU	Multiple Bit Upset
NASA	National Aeronautics and Space Administration
NC	Neuromorphic Computing
PSP	Postsynaptic Potential
RHBD	Radiation Hardening By Design

SDC Silent Data Corruption

SEL Single Event Latchup

SEE Single Event Effect

SEU Single Event Upset

SET Single Event Transient

SIPP SEU Induced Parameter Perturbation

SNN Spiking Neural Network

SoC System-on-Chip

SPE Solar Particle Event

SPENVIS Space Environment Information System

SWaP Size, Weight and Power

TID Total Ionizing Dose

TMR Triple Modular Redundancy

VLSI Very Large-Scale Integration

Abstract

The number of satellites in orbit is increasing at an accelerating pace. One major issue that currently hinders the range of satellite applications is data analysis. Most data is transmitted back to ground stations for analysis resulting in bandwidth-related issues, or the processing is performed on board, necessitating large computational power. Spacecraft, particularly miniaturized ones, face stringent energy constraints due to the scarcity of resources and the harshness of the space environment. Processing data at the edge using Spiking Neural Networks (SNN) applied on mixed-signal Neuromorphic Computing (NC) processors has been proposed as a potential solution. Neuromorphic devices focus on low power and energy-efficient operation, which aligns well with the requirements of space applications. Nevertheless, the response of these devices to the harsh conditions of the space environment remains only partially understood. The primary uncertainty lies in the impact of cosmic radiation, which can present substantial challenges, even in low orbits. Radiation not only has the potential to damage hardware but also to interfere with its operation, leading to potentially detrimental software failures. The objective of this work is to describe and analyze the effects of space radiation on NC processors. A behavioral model of different types of radiation effects is composed and experimental verification is performed at a proton beam facility using a mixed-signal NC prototype. The radiation effects are analyzed, and their influence on network operation is discussed. It is demonstrated that mixed-signal NC is resistant to perturbations caused by radiation. Additionally, software mitigation strategies are proposed to further increase the applicability of SNNs in radiation environments.

1 Introduction

The number of satellites being launched every year is increasing, with the most notable increase in small satellites (SmallSats) [1]. The production of small but capable satellites with mass classes considerably below 10 kg has been made possible by the shrinking of processing systems for Earth Observation (EO) [2, 3]. However, the up-and-downlink bandwidth, onboard computer power, and ground station availability still represent major issues limiting the development and operation of remote sensing missions, especially for miniature spacecraft. For example, the maximum downlink throughput is directly affected by the limited system power budget resulting from small solar panels and batteries often found in SmallSats [4].

To examine potential bandwidth advantages from data processing at the edge, the use of Artificial Intelligence (AI) onboard spacecraft has been studied [5, 6, 7]. The deployment of value-added applications in space using a minuscule fraction of the downlink bandwidth would be possible thanks to AI-based architectures for EO satellites that embed AI algorithms, such as a Deep Neural Network (DNN), for consuming data at the source rather than on the ground. Thus, large quantities of data, for example, in hyperspectral imaging, can be processed onboard using AI before being sent to Earth [8]. However, running DNNs generally requires a significant amount of power, and conventional space hardware is not suitable for efficiently employing these networks [9].

One possible approach to achieve neural network operation with minimal power consumption is through the utilization of Neuromorphic Computing (NC) [10]. These computers possess a non-Von Neumann architecture, resembling that of a biological brain, enabling them to carry out computations with exceptional efficiency. Furthermore, NC has the ability to utilize analog signals instead of digital ones, leading to an even greater reduction in power consumption for computations. Therefore, the use of analog NC processors could potentially enable the widespread application of AI in space [11, 12]. Also, for planetary exploration applications, the power efficiency of NC systems could provide a solution to future problems [13].

One drawback of processing data in space is that electronic devices are susceptible to space radiation leading to errors or system failure [14]. Much research has been conducted to analyze these effects in conventional electronic systems in space [15, 14]. However, how radiation effects might influence analog neuromorphic processors has not been well characterized. However, certain studies suggest that NC could potentially exhibit higher fault tolerance compared to traditional architectures, making it a more suitable choice for applications in space. [16, 17].

This research investigates the radiation effects that might occur in NC systems and find mitigation strategies to increase their fault tolerance. In chapter 2, the state-of-the-art in several related research fields is analyzed. Also, the interaction between these separate fields is made clear. Next, the goals of this research are provided, along with several research questions in chapter 3. Relevant background information that serves as a basis for this research is provided in chapter 4. In chapter 5, the method that will be applied during the research and the setup used for conducting experiments are described.

chapter 6 describes the found radiation effects and the effectivity of applying different mitigation strategies. Limitations of the research as well as improvements for future work, are mentioned in chapter 7. Finally, conclusions are formulated in chapter 8 based on the results from simulations and experiments, and their potential significance is described.

During this research, sensitive information relating to intellectual property has been used to produce a model and obtain simulation and experimental results. The sections that include this information are grouped in Appendices A and B. These sections are referred to throughout the report. In the public version of the report, these appendices will be removed in order to prevent the disclosure of sensitive information. Furthermore, the graphs presented in this report have undergone modifications to ensure that specific hardware details cannot be inferred.

2

Literature Review

In this section, the current state-of-the-art with respect to processors in radiation environments is discussed. In section 2.1, the current efforts regarding advanced computation in space are described. Next, the potential benefits of neuromorphic processors are introduced in section 2.2. Consequently, the operational environment and the errors resulting from radiation are provided in section 2.3. In subsection 2.3.6, possible strategies for mitigating radiation susceptibility are briefly described.

2.1. Advanced Computation in Space

In the past, space technology has typically provided limited computing power in comparison to contemporary Earth-based systems. However, there has been a recent shift towards employing more Commercial-Off-The-Shelf (COTS) processors in space applications. Presently, there is a substantial endeavor to develop enhanced flight computers capable of effectively handling the increasing demand for onboard processing and image detection [18]. Also, COTS processors such as the Intel Movidius Myriad 2, Myriad X, NVIDIA Jetson NANO and Qualcomm Snapdragon 855 are currently used in space because they provide significant computing power in a small Size, Weight and Power (SWaP) package [19, 9, 6, 7]. These systems enable direct hardware acceleration for DNNs that can be applied onboard satellites, the Mars Ingenuity Helicopter, and other space drones [9, 19]. Operation of these space assets for onboard data analysis, increased autonomy, and targeted downloads, is made possible with edge processing [9]. There is currently a significant effort to develop improved flight computers capable of managing the growing need for onboard processing and image detection [18]. Even though these systems are all still based on conventional computer systems, some novel initiatives also focus on neuromorphic solutions for space applications [20, 21, 17, 22]. These neuromorphic systems are aimed at the application of a Spiking Neural Network (SNN) rather than a conventional Artificial Neural Network (ANN) or DNN. SNNs have potential advantages, such as energy efficiency, efficient result uncertainty estimation, and strong performance on event-based data, which make them promising for data processing in autonomous operations [23, 16]. Thanks to recent advancements in architectures and training techniques, SNNs have reached a level of performance that is comparable to that of ANNs in numerous tasks [24, 25, 26, 23]. However, it is unclear how SNNs compare to ANNs in terms of energy, latency, and performance trade-offs when applied to tasks using static data such as the classification of EO images [27]. For example, studies indicate that the energy and performance benefits of SNNs for data sets with complex features can strongly depend on the method used to encode information [26, 28]. Therefore, the complexity of features often found in satellite data could pose a challenge for SNNs. The Advanced Concepts Team of the European Space Agency (ESA) is currently evaluating and comparing SNNs and ANNs for onboard scene classification [17].

2.2. Neuromorphic Computing

Conventional computer systems use a Von-Neumann architecture containing a Central Processing Unit (CPU), where computations are performed, and a memory, where results and parameters are stored. The connection, or ”bus”, between these units can pose a restriction on the amount of data that

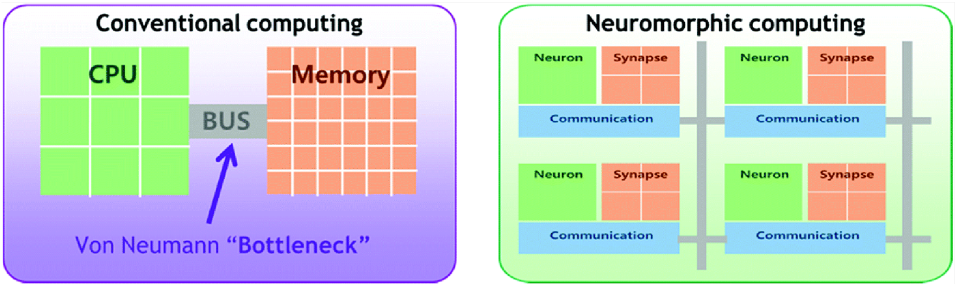

Figure 2.1: A graphical representation of the differences between a Von-Neumann and NC architecture [29]. The Von-Neumann bottleneck, a constraint on the amount of information that can flow between memory and CPU, is also indicated.

can be processed due to the limited frequency of read/write operations. Contrarily, NC architectures resemble the structure and operation of biological brains [30]. These systems are comprised of neurons and synapses, and memory is decentralized instead of located in one specific section [31]. The difference between a conventional Von-Neumann architecture and NC systems is represented in Figure 2.1.

A neuron or synapse consists of a small Integrated Circuit (IC) that can process electric signals in parallel to the other ICs to perform large amounts of calculations at high speed. The behavior of neuromorphic neuron and synapse hardware implementations tends to be simplified with regard to biological brain cells unless the goal is to model the complicated biological behavior in detail [32, 33, 34]. Even though there exist many different levels of the intricacy in the electrical behavior, some general concepts apply for NC neurons and synapses. Neurons have a threshold mechanism that allows them to respond to incoming signals in a non-linear manner. Only if the combination of incoming signals exceeds the neuron threshold does the IC generate an action potential resulting in an output signal [34]. Synapses are specialized terminals that enable neurons to communicate with one another through the exchange of these input and output signals. Multiple instances of these ICs can be integrated onto NC chips using Very Large-Scale Integration (VLSI) and connected to form networks. The level of connectivity required for a network implementation is determined by the desired functionality of the system [35].

The main advantages of NC with respect to conventional computing are increased processing speed, the removal of the memory bottleneck, and decreased power consumption [35]. These characteristics make NC very suitable for running neural networks such as DNNs that require large amounts of parameters and processing power. However, there are also some disadvantages to NC, such as the absence of powerful development tools [16].

Many different NC hardware implementations exist, which can generally be divided into analog and digital NC implementations [35]. Determining whether analog or digital implementations are superior to each other is challenging because both have their strengths and weaknesses. As a result, they are frequently combined in a single ”mixed-signal” processor. A brief overview of a number of real-life NC systems is provided in Table 2.1.

For embedded applications in space, only a few existing neuromorphic systems are usable. Since (mixed-signal) NC is still mainly a focus of research, no exploration has been made into designing such systems to resist space radiation. However, prominent industrial parties, including ESA, National Aeronautics and Space Administration (NASA), and the United States Air Force, are presently engaged in addressing these challenges [17, 16, 36, 37].

2.3. Space Radiation

The radiation environment in space is heterogeneous both temporally and spatially. The majority of space missions, such as those involving EO and planetary exploration, take place within our solar system. Therefore, the radiation environment in this region will be studied. In the solar system, the most dangerous radiation for electronics consists of ionizing particles emitted by the Sun, coming from Galactic Cosmic Rays (GCR), or those found in so-called radiation belts.

Company/Lab	Chip type	#Neurons/ synapses	Power	Software	Applications
ROLLS	Mixed-signal	256/64K	∼5mW	Custom python	Research
DYNAP-SE	Mixed-signal	4K/4M	∼5mW	Custom python	Research
NeuroGrid / Stanford	Mixed-signal	1 M/billions	∼3W	NEF	Real-time SNN emulation
Innatera	Mixed-signal	256/64K	∼1mW	Talamo, PyTorch	Smart sensing
BrainScaleS 1/ Universität Heidelberg	Mixed-signal	∼180,000/ 40M (in 352 chips)	∼300W	BrainScaleS OS	Research
BrainScaleS 2/ Universität Heidelberg	Mixed-signal	512/ ∼130,000	∼1W	BrainScaleS OS	Edge processing, robotics
TrueNorth / IBM	Digital	1M/ 256M (in 4K cores)	∼0.3W	Custom	DNN acceleration
SpiNNaker / University of Manchester	Digital	1B/10 kilobytes (in 64 K x 18 ARM cores)	∼kW	PyNN, NEST	Research
Loihi / Intel Labs	Digital	∼128,000/ 128M per chip (scalable)	∼1W	Lava	Research
Dynap-CNN / SynSense	Digital	∼327,000/ 278,000	∼5mW	Rockpool, PyTorch	Smart sensing
BrainChip / Akida	Digital	Configurable, 8-Mb SRAM	∼30mW	TensorFlow	Smart sensing, one-shot learning
Tianjic / Tsinghua University	Digital	40,000/10 M (on 156 cores)	∼1W	Custom	ANN/SNN acceleration

Table 2.1: A collection of NC systems with their main characteristics [38]. Sources for ROLLS [39], DYNAP-SE [40], Innatera [41], NeuroGrid [42], BrainScaleS 1 [42] and 2 [43, 44], TrueNorth [45], SpiNNaker [46], Loihi [47] and Tianjic [48].

2.3.1. Solar Particles

The sun emits radiation in two forms: the solar wind and solar particle events; where both consist mainly of protons and electrons. Due to its low energy, solar wind is not a concern for space electronics, but solar particles are more energetic and can therefore be harmful [49]. The temporal variation of the flux of solar particles is dependent on the solar cycle of ∼ 11 years and solar activity linked to Solar Particle Event (SPE)s. These events can happen 50 times in a single solar cycle, with an extremely variable frequency that is generally higher during the solar maximum [50]. SPEs can be divided into two categories: the Coronal Mass Ejection (CME) or the impulsive solar flare. SPEs connected to impulsive solar flares are brief, typically lasting a few hours, and are distinguished by comparatively significant electron fluxes. Overall energetic particle fluence is between 10^7 and 10^8 particles per cm^2, and these events are restricted to a 30° to 45° angle in solar longitude. SPEs linked to CMEs, have a lifespan on the order of days, a proton fluence that can exceed 10^9 particles per cm^2 and can spread over a broad angle in solar longitude extending from 60° to as much as 180° [50].

2.3.2. Galactic Cosmic Rays

GCRs primarily consist of heavy ions, whose energy can range from a few MeV up to tens of GeV, that pose a significant threat to biological and electrical structures due to their high energy [51]. The distribution of these particles is isotropic in (interstellar) space and considerably lower in quantity compared to the particles emitted during SPEs. Additionally, the flux of GCRs is influenced by factors such as the solar cycle (as shown in Figure 2.2) and magnetic fields, including Earth's magnetic field [49].

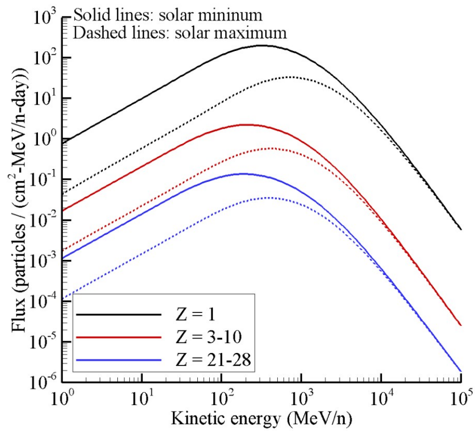

Figure 2.2: The flux of GCRs in the solar system for solar minimum and solar maximum according to recent radiation models [52]. The letter Z indicates the atomic number of the heavy ions.

2.3.3. Earth's Radiation Belts

The Earth's Radiation Belt (ERB)s are toroidally-shaped regions where particles from the Sun and GCR are trapped due to interaction with the geomagnetic field. There are two of there regions near Earth: the inner belt consisting mostly of protons and the outer belt consisting mostly of electrons [53]. These regions pose a threat to spacecraft that traverse them. Depending on the exact orbit and solar cycle, a spacecraft will encounter these radiation environments in varying degrees during its lifetime [49]. A basic overview of the radiation environments near Earth and the radii of some common satellite orbits are shown in Figure 2.3.

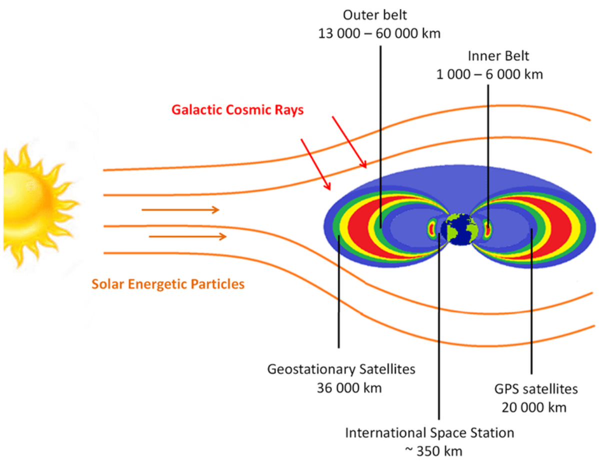

Figure 2.3: Schematic representation of radiation sources [54]. The red areas in the ERBs are indications of large particle concentrations.

2.3.4. Radiation Models and Tools

The radiation environments mentioned in the previous section have been captured in models for space environment analysis. The most recent models are quickly highlighted here as they could be used for estimating the level of particle interaction that electrical hardware may be subjected to in space.

Several mathematical en semi-empirical models of the GCR flux have been developed over the last several decades. Recent versions of these, such as the Badhwar and O'Neill model [55] presented in Figure 2.2 and the Nymmik model [56] are incorporated in the web-based CREME96 program [57].

For modeling the particle abundance in the ERBs, the AP-8 proton and AE-8 electron maps have served as the primary foundation for decades [53]. These models have been surpassed by the more recent AP-9 and AE-9 models, which are also accessible online [58]. A visualization of these is provided in Figure 2.4.

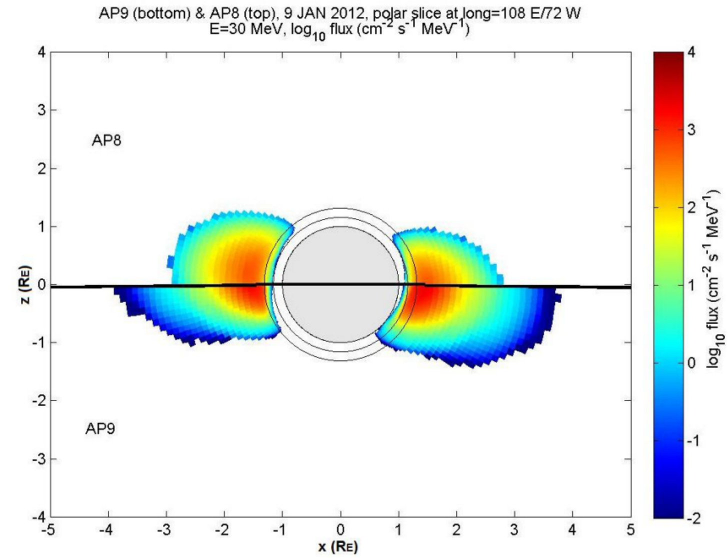

Figure 2.4: The spatial distribution of trapped protons according to the NASA AP-9 model compared to the AP-8 model [59]. The units on the x and y-axis are Earth radii (roughly 6371 km).

Space Environment Information System (SPENVIS) is a valuable tool that combines several radiation models. It allows the user to input precise orbits and mission profiles. Also, parameters such as shielding can be incorporated. Consequently, it can calculate results such as encountered particle fluxes and spectra as seen in Figure 2.5. These results can then be combined with the spacecraft hardware characteristics to estimate the level of radiation-induced effects that may be experienced for a specific orbit.

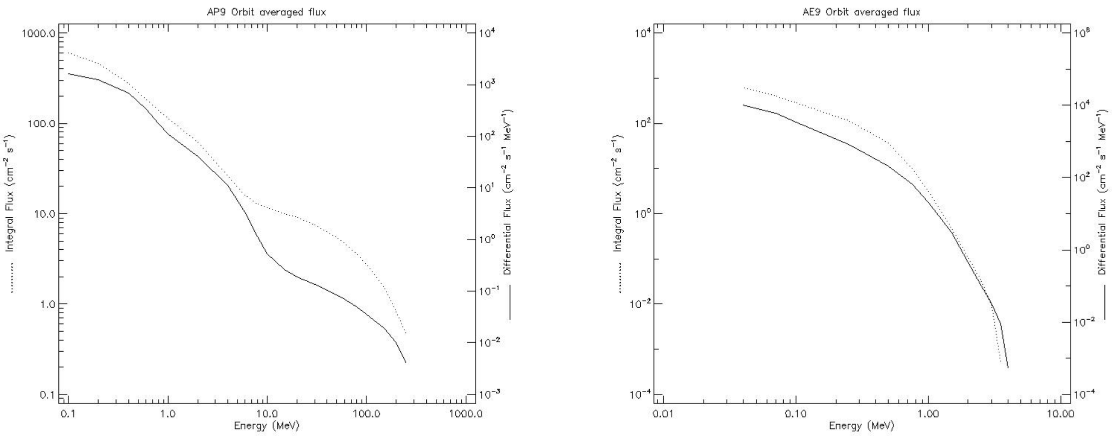

Figure 2.5: AP-9 trapped proton (left) and AE-9 trapped electron flux (right) for a 300-750 km Low Earth Orbit, with an inclination of 10 degrees, generated using SPENVIS.

2.3.5. Radiation and Spacecraft

Radiation influences the operation of electronics by physically interacting with the hardware. The type of interaction depends largely on the characteristics of the impinging particles [60]. A common distinction is made between a Single Event Effect (SEE), Total Ionizing Dose (TID), and Displacement Damage (DD). A visual representation showing what types of radiation cause these effects is presented in Figure 2.6.

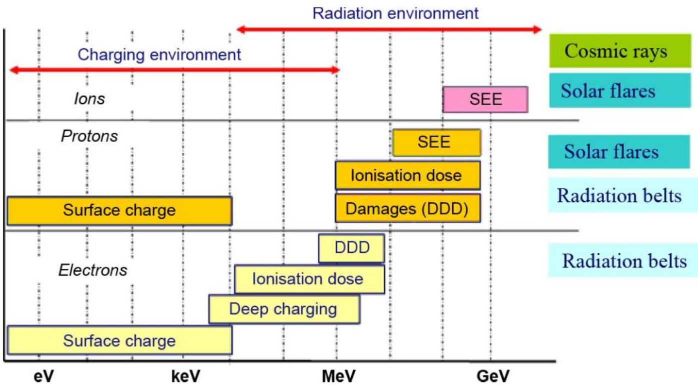

Figure 2.6: The various sources of space radiation are listed along with their most common effects on electronics [14].

For this research, only the effects caused by ionizing radiation (i.e., SEE and TID) are considered, as these are more likely to result in measurable deviations from nominal behavior in processors and often lead to functional anomalies in spacecraft [14]. An overview of these errors and the number of occurrences in some space missions is provided in Figure 2.7. The basic theoretical mechanisms of radiation interactions and any effects they may cause in delicate electronics are described further in section 4.3.

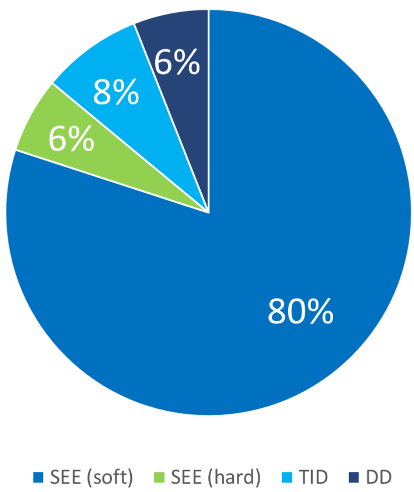

Figure 2.7: Occurrence of different radiation effects for over 100 anomaly cases [14]. A distinction is made between hard (destructive) and soft (non-destructive) SEEs.

2.3.6. Radiation Mitigation

Generally, radiation effects on spacecraft electronics are mitigated using three main strategies: shielding, radiation hardening, and error correction [49]. Each of these strategies has its advantages and disadvantages, and how to combine them depends on the radiation circumstances and mission requirements [61].

Shielding involves placing a substance between sensitive hardware and incoming radiation to attenuate the radiation reaching the device. However, this often results in additional weight leading to cost increases for space applications. Radiation hardening can be achieved through changes in the design of the electrical circuits, also called *Radiation Hardening By Design (RHBD)*, or pre-processing hardware in such a way that radiation effects are less likely to occur. This complicates the hardware production process leading to a higher cost for radiation-hardened products such as processors. Error correction aims to detect and correct the errors or perturbations that occur in electronic devices due to the occurrence of radiation effects. This is generally done by incorporating redundant hardware (e.g. additional memory) or software (e.g. performing calculations multiple times) in the system. Modern Error Detection and Correction (EDAC) or Error Correcting Code (ECC) protection can reduce device failure rates by over 10,000 times, but it often requires extra memory, more computational power, and causes operational delay [62, 61]. For this research, only software mitigation strategies are investigated.

3

Research Goals and Questions

In this chapter, the most important research questions are proposed based on the current state-of-the-art described in chapter 2. The research is considered complete when these questions are answered.

3.1. Research Goal

From the literature review, several gaps have been identified in the scientific knowledge. As demonstrated, mixed-signal NC processors form a promising technological advancement in low-power AI applications. Similarly, it has been shown that these AI operations have potential added value in space missions. However, no neuromorphic system has been demonstrated in space. This is partly due to the risk-averse space industry and the relatively early stages of NC development. Another distinguishable caveat of mixed-signal neuromorphic systems is the fact that these have not yet been tested for radiation sensitivity as opposed to conventional computer architectures. Also, mitigation strategies for this type of hardware accelerator have not been investigated yet. Since it has been demonstrated that space radiation is a factor that must be incorporated in the design of successful space-embedded systems, filling these knowledge gaps can contribute to accelerating the development of NC processors for space applications. This is, therefore, the main goal of this research.

3.2. Research Questions

The main question that is answered in this research is:

> ”How can radiation effects in mixed-signal neuromorphic processors be mitigated to enable reliable spiking neural network applications in space?”

This question describes the exact gap in the current scientific knowledge regarding the application of NC processors in space. To provide an answer to this question, multiple sub-questions are also relevant. The goal is to find meaningful answers to these questions that allow the main research question to be answered.

Label	Research questions
RQ-1	**How sensitive are mixed-signal neuromorphic processors to radiation?**
RQ-1.1	How can SEEs be modeled in mixed-signal neuromorphic processors?
RQ-1.2	How can TID be modeled in mixed-signal neuromorphic processors?
RQ-1.3	How can a model describing SEEs in mixed-signal neuromorphic processors be validated?
RQ-1.4	How can a model of TID effects in mixed-signal neuromorphic processors be validated?
RQ-1.5	How does error propagation differ between mixed-signal NC processors and digital Von-Neumann architectures?
RQ-2	**How can radiation effects on mixed-signal neuromorphic processors and their effect on SNN operation be mitigated?**
RQ-2.1	How can SNNs be made fault-tolerant for radiation-induced perturbations?
RQ-2.2	How can strategies for mitigating radiation-induced errors in mixed-signal neuromorphic processors be validated?

Table 3.1: The main questions with relevant sub-questions for this research.

3.3. Research Structure

The research comprises several distinct stages that were undertaken progressively. Initially, a gathering of theoretical background knowledge was conducted, focusing on the modeling of radiation effects in an IC. Subsequently, the necessary simulation software and models were developed to assess how radiation could induce deviations from the expected behavior in SSNNs. This knowledge formed the basis for formulating a systematic experimental approach to fine-tune and validate the radiation models. Proton beam experiments and a mixed-signal NC prototype were employed to collect experimental results. After the validation phase, mitigation strategies were implemented in the simulated networks to enhance the fault tolerance of the utilized SNNs.

4

Theoretical Framework

In this chapter, the theoretical concepts and models that underpin the research are explained. Firstly, the focus is on discussing SNNs and clarifying their differences from NC processors. Furthermore, the theory regarding radiation effects on sensitive electronics and their underlying mechanisms is provided.

4.1. Spiking Neural Networks

SNNs can be described as a class of neural networks where neurons transmit information to other neurons via synapses using discrete spike patterns. In this section, the fundamental building blocks that are used in an SNN are described. Subsequently, a simple model is presented to explain the working principle of a network consisting of neurons and synapses.

4.1.1. Neurons

To describe the functioning of SNNs, a fully-connected recurrent SNN consisting of a number *N* neurons and *S* synapses can be considered. The fan-in and fan-out of each neuron are $N-1$. Many electrical parameters can be used to achieve detailed neuronal behavior but every neuron has the following basic properties:

- Threshold voltage: the membrane voltage at which the neuron fires.
- Reset voltage: the voltage that the neuron membrane potential resets to after firing (generally *0* V).

A Leaky-Integrate-and-Fire (LIF) neuron, which is often applied in SNNs, regulates its membrane potential according to the following equation:

$$\frac{dV_{mem}}{dt} = \frac{i_{bias} + i_{leak}}{C} + Q_{total} \tag{4.1}$$

Where V_{mem} is the membrane voltage, i_{bias} is the current supplied to the neuron, i_{leak} is the leakage current which always draws the membrane voltage towards zero, t is the time, C is the capacitance of the neuron and Q_{total} is the sum of the synaptic charge.

4.1.2. Synapses

Synapses are used to exchange signals between individual neurons. The amount of synapses, assuming one neuronal branch with a single synapse between each neuron, is equal to N^2. This number could be higher by employing redundant synapses, also called *multapses*. Generally, synapses have the following basic properties:

- Synaptic weight: an indicator of the strength of the connection between the presynaptic and postsynaptic neuron. A negative weight results in an Inhibitory Postsynaptic Potential (IPSP) and a positive weight in an Excitatory Postsynaptic Potential (EPSP).

- Synaptic delay: a delay between the arrival of a presynaptic spike and generation of a Postsynaptic Potential (PSP).

Again, more parameters can be added to the synapse to obtain more intricate temporal behavior. For a current-based synapse implementation, a PSP is generated according to:

$$\frac{di_{syn}}{dt} = -\frac{i_{syn}}{\tau_{syn}} \tag{4.2}$$

Where i_{syn} is the synaptic current and τ_{syn} is the synaptic time constant. To find the amount of charge injected into the postsynaptic neuron by a single spike, we can solve the differential equation:

$$i_{syn} = wI_0 e^{-\frac{t}{\tau_{syn}}} \tag{4.3}$$

Where w is the synaptic weight and I_0 the unit synaptic amplitude. Consequently, the charge per spike can be found by evaluating the integral from 0 to infinity:

$$Q_{syn} = wI_0\tau_{syn} \tag{4.4}$$

The total charge for a given number of input spikes N_{in} is:

$$Q_{total} = Q_{syn} \cdot N_{in} \tag{4.5}$$

The amount of charge transferred between neurons for a given input can be regulated by tuning individual synaptic weights. Using various training methods similar to generic ANNs, the SNN can be trained to perform specific functions with the input.

4.1.3. Working Principle

To operate an SNN, a series of spike inputs need to be sent to the network. This can be done by encoding information as spikes as presented in Figure 4.1.

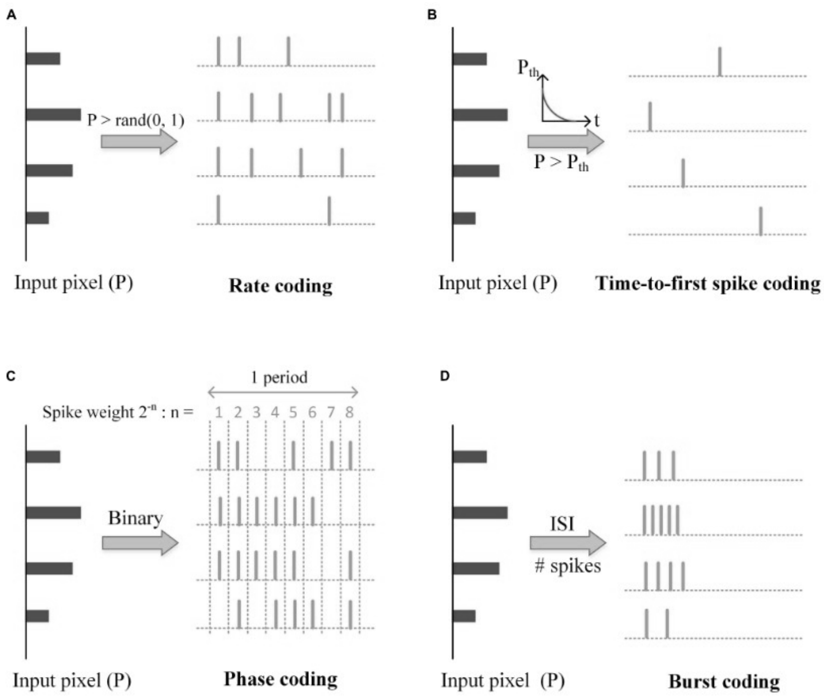

Figure 4.1: A graphical representation of commonly used encoding schemes in SNNs [63].

These spike sequences can be used as input to an SNN. A schematic representation of a basic SNN employing LIF neurons is presented in Figure 4.2.

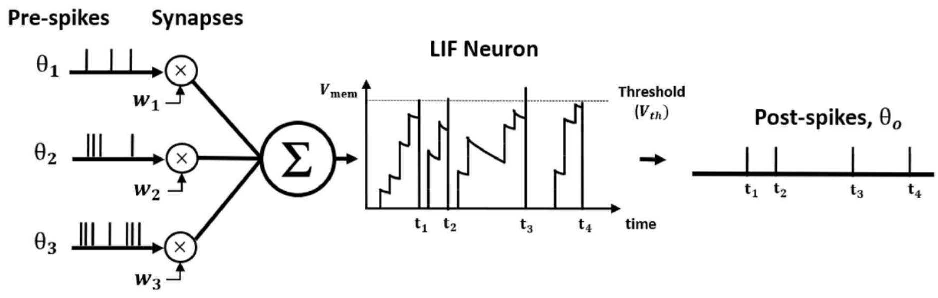

Figure 4.2: A schematic representation of a LIF neuron with 3 presynaptic neuron input spike sequences [64]. These spikes are modulated by their respective synaptic weight w_n to obtain PSPs which are summed and integrated into the membrane voltage V_{mem} of the postsynaptic neuron. Every time the threshold V_{th} is reached, an output spike is produced, and the membrane voltage resets.

After an input spike volley has propagated through the network, it can be encoded back into useful information for further processing.

4.2. Neuromorphic Computing

Neuromorphic computing has many resemblances to SNNs. Both consist of neurons and synapses and can perform computations using sequences of spikes. However, NC processors differ in the fact they are made up of physical hardware compute elements (either digital or analog), whereas an SNN is only a theoretical model that can be implemented in practically any digital computer. The subsequent sections elaborate further on this distinction.

4.2.1. Neurons

For analog representations of biological neurons, activity is described by a set of equations that can be either very extensive such as the Hodgkin-Huxley (HH) neuron, or very simple such as the McCulloch-Pitts model [65, 66]. The selection between the two implementations is a trade-off between circuit size and the intricacy of temporal dynamics. Given the intricacy of biological neurons, a sizable silicon area and several bias voltages or currents are necessary to accurately reproduce their function. Compared to more complicated models, simplified LIF models often need fewer transistors and parameters, but they frequently struggle to mimic the diverse range of biological actions [33, 34]. However, these are advantageous for VLSI implementations due to their computational simplicity and compactness [67, 68].

4.2.2. Synapses

Synaptic circuits convert presynaptic voltage pulses into postsynaptic currents injected into the membrane of the postsynaptic neuron. Dedicated sub-threshold analog circuits can effectively perform this function, emulating intricate synaptic dynamics [69]. Similar to VLSI neurons, the behavior of VLSI synapse implementations also tends to be simplified unless the goal is to model the complicated biological behavior in detail [32]. Moreover, synaptic realization in hardware is subject to a number of significant physical constraints, as opposed to theory or software simulation. For instance, the precision of synaptic weights is constrained, and their range of values is bounded. The learning capacity of the SNN using such synapses is significantly impacted by these constraints [70, 71].

4.2.3. Networks

The silicon neuron and synapse circuits can be combined together to form fully functional neural networks. Multiple VLSI implementations of these elements can be integrated onto chips and connected among each other with on-chip or off-chip connections that can either be hard-wired or re-configurable. Different network topologies can be desired for an NC system. Determining the level of connectivity that is required for a network implementation and then finding the appropriate hardware that can accommodate that level of connectivity is often a non-trivial exercise. This largely depends on whether the goal is to replicate biological behavior closely or to allow a certain degree of functionality using interconnections that allow for easy learning [35]. These functional systems could benefit from a large fan-in and fan-out or even a fully-connected network and then using learning to isolate the correct interconnections. This is the general approach applied for multi-purpose NC hardware.

4.3. Radiation Effects

The main effects that radiation can have on computer processors are described in this section. A schematic representation of the theoretical mechanisms causing SEE and TID is provided in Figure 4.3.

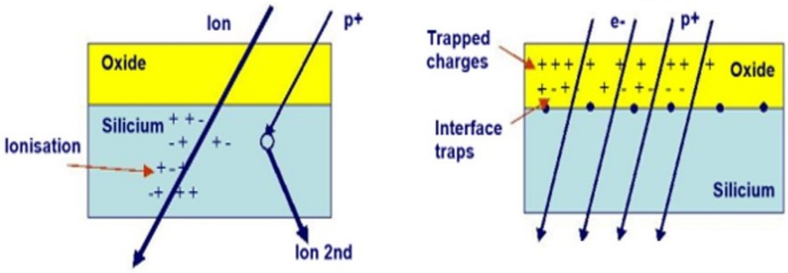

Figure 4.3: The physical interaction with ionizing particles in SEEs (left) and TID (right) [1].

4.3.1. Total Ionizing Dose

The term TID describes the result of a long-term, homogeneous buildup of (small) ionizing dose depositions in insulators and oxides as shown in Figure 4.3. The duration of exposure of the target device to incoming space radiation has a significant impact on the TID effects, which are primarily caused by interactions with protons and electrons. The amount of TID can be calculated using the characteristics of the circuit and the stopping power of the incoming particles in the target material. The stopping power S is the amount of energy E lost by the particle per unit length x:

$$S = \frac{dE}{dx} \tag{4.6}$$

This stopping power can then be used to calculate the amount of deposited dose:

$$D = \frac{1}{\rho} \int_{E_1}^{E_2} \phi(E) \frac{dE}{dx}(E) dE \tag{4.7}$$

where ρ is the mass density of the target material and $\phi(E)$ is the differential energy spectrum defined between E_1 and E_2. The International System unit is Gray: 1 Gy = 1 J/kg, although rad (radiation absorbed dose) is also frequently used: 1 Gy = 100 rad [72]. While it is possible to estimate the deposited dose to some extent using theoretical calculations, predicting the electrical effects on the device is significantly more challenging. Generally, the defects will modify the threshold voltage and change the mobility of the gate and field oxide [73]. As a result of these effects, accumulation of dose leads to parametric degradation of the electrical performance of electronic devices [51].

4.3.2. Single Event Effects

Single event effects are caused by a sudden (large) ionizing dose deposition, from a single particle, in a sensitive region of the device [15]. If the particle energy is sufficiently high, electrons in the atoms of the target medium can interact with incoming protons and heavy ions. These electrons are consequently pulled out of the orbit around the nucleus and released. As shown in Figure 4.3, there are two basic mechanisms for SEEs:

- An incident heavy ion causes- an ionization track in a sensitive region in the device resulting in an amount of charge being collected in the device. Generally, an incoming heavy ion leads to SEE more often than an incoming proton [15].

[1]Retrieved from: `https://easii-ic.com/en/radiation-tests` on 13/04/2023.

- An incident proton transfers its energy to a recoil atom in the target medium through collision or destruction of the nucleus. The recoiling nucleus deposits energy in the same way as a heavy ion but has a shorter range. The probability of a proton undergoing such a reaction is low (approximately 0.001% for most devices); however, the flux of protons in space can be so large that this mechanism can dominate the SEE rates in many situations [74].

The types of SEEs are numerous, but they can generally be separated into hard (destructive) and soft (non-destructive) errors. These soft errors are all basically bitflips, but based on the location in the system, they are categorized differently. The instantaneous perturbation caused by the charged particle leads to functional anomalies in most kinds of electronic devices [14, 49, 51]. A short overview of different types of SEEs is given in Table 4.1 and Table 4.2.

SEE name	Effect in electronic component
Single Event Latchup	High current spike
Single Event Snapback	High current spike
Single Event Burnout	Destructive burnout
Single Event Gate Rupture	Rupture of gate dielectric

Table 4.1: Examples of hard errors [51].

SEE name	Effect in electronic component
Single Event Upset	Corruption of information in a memory element
Multiple Bit Upset	Corruption of information in several memory elements
Single Event Functional Interrupt	Loss of normal operation
Single Event Transient	Impulse response of certain amplitude and duration
Single Event Disturb	Momentary corruption of the information in a bit

Table 4.2: Examples of soft errors [51].

5 Methodology

In this chapter, the simulation and experimental setup are discussed, along with the parameters and the metrics used to achieve and evaluate results. Also, the techniques used to mitigate the radiation effects in mixed-signal NC processors and the rationale behind the approach are explained.

5.1. Simulation setup

The simulation setup is discussed here, starting with the systems engineering approach, and provides details with respect to relevant model parameters and an explanation of software settings.

5.1.1. Simulation Requirements

The goal of simulating the networks that are implemented on the prototype is to find potential ways in which radiation might influence the output of a network before testing and to assess the effectiveness of hardware-agnostic mitigation strategies applied after experimental verification. To fully address the requirements the simulation has to adhere to, Table 5.1 was composed.

Label	Requirement
SIM-1	The simulation shall be able to model at least the same number of neurons and synapses as the Innatera prototype.
SIM-2	The simulation shall be capable of changing the type of neuron model.
SIM-3	The simulation shall simulate the timing and propagation of spikes and synaptic events with high accuracy.
SIM-4	The simulation shall simulate the timing and propagation of spikes and synaptic events with high repeatability.
SIM-5	The system shall be able to simulate different types of synaptic connections, including excitatory and inhibitory connections.
SIM-6	The simulation shall be able to incorporate external input.
SIM-7	The simulation shall provide visualization tools to allow researchers to explore and analyze the network activity, such as displaying raw spike plots, membrane voltages, and connectivity diagrams.
SIM-8	The simulation shall record and store simulation data, including spikes, synaptic weights, and network activity over time, for further analysis.
SIM-9	The simulation shall be able to simulate the effects of different types of perturbations on the network, such as noise, damage, or parameter changes, to allow for the testing of hypotheses.
SIM-10	The simulation shall be numerically stable.

Table 5.1: Simulation requirements

5.1.2. Simulation Software

In order to experiment with SNNs, it is necessary to have a suitable simulator environment that can interact with the model and simulate the behavior of intricate, large-scale neural networks. Several options for simulators exist, such as Brian2 [75], NEURON [76], and NEST [77]. Additionally, Python libraries, such as PyNN, enable the fabrication of simulator-independent SNNs. For this research, Brian2 was selected because it satisfies the necessary requirements mentioned in Table 5.1 while also being easy and flexible to use [78].

Brian2 is a simulator that allows researchers to simulate SNNs with ease and efficiency, including custom dynamical equations, interactions with the environment, and experimental protocols. Unlike other simulators that require low-level programming, Brian2 automatically generates efficient low-level code based on high-level descriptions of models. This approach avoids the need for expertise in low-level programming and ensures the reproducibility of computational experiments, even when they include complex stimulation procedures. After simulation, data relating to spikes, network parameters, or individual neuron dynamics can be extracted and converted into many conventional Python data structures, which can be used for visualization and further analysis.

Simulation Parameters

The simulation parameters determine the duration and resolution of the simulated network operation. This includes the time step used for simulating the electrical signals in the neurons and synapses. For the simulations, a time step of 0.5 microseconds was used to allow for sufficient resolution of signals while also enabling fast computation. The Runge-Kutta (RK4) integration method was chosen as it strikes a good balance between accuracy, efficiency, ease of implementation, and stability.

Synapse Parameters

The synapse parameters determine how a presynaptic spike is converted to a PSP. The most important parameters are the synaptic weight and the synaptic time constant. The weight determines the height of the PSP, and the time constant determines the width of the PSP. Both of these influence the membrane potential of the postsynaptic neuron. The impact on the membrane potential of the postsynaptic neuron becomes more pronounced as the weight increases. While weights can be assigned any value, in this case, they were assigned identical values to the Innatera prototype. The parameters for the synapses are listed in Table 5.2.

Neuron Parameters

Finally, neuron parameters determine the (temporal) behavior of the simulated neurons. The neurons were modeled with LIF behavior adherent to Equation 4.1. For this research, the neurons on the Innatera prototype can be employed in a similar manner to general LIF neurons. Extreme cases where this similarity is no longer true are avoided in the experiments.
Although it is possible to simulate a perfectly behaved network by providing all neurons with the exact same parameters, this does not accurately reflect the analog neurons found in the Innatera prototype. These neurons are comprised of uncalibrated integrated circuits as mentioned in chapter 4, where a small amount of variation between the networks is expected. Therefore, the neuron capacitance is initialized using a Gaussian distribution with a fixed standard deviation. As a result, spiking frequencies differ slightly between neurons. Also, a stochastic parameter is added to simulate Gaussian white noise in the membrane voltage. To ensure stable simulation, it is common practice to model the noise as an Ornstein-Uhlenbeck process, which has also been employed in this case [79]. The parameters for the neurons are listed in Table 5.2.

5.2. Model Verification

In this section, it is verified that the simulation model is correctly implemented and performs as expected. It involves checking that the model is free of mathematical errors, consistent with theoretical LIF models, and capable of producing results that align with expectations. To confirm that the simulation accurately implements the mathematical models for neuron and synapse behavior, several tests are performed.

5.2.1. Physical Units

To ensure that the simulation does not contain any coding errors, a check of the physical units is performed. Quantities and equations in Brian2 can be modified to use SI units. The software automatically verifies that the operations on units are consistent and will generate an error for any dimensionality mismatches. No errors are reported in the simulation, indicating the correct handling of quantities in the physical equations.

5.2.2. Bias Current

To check if the simulation's outputs are consistent with the expected outputs given the input data, an analytical calculation of the membrane voltage has been compared with the response of a single simulated neuron. In this case, the analytical model shows the ideal neuron behavior if the neuron is given a steady-state bias current as described by Equation 4.1. The similarity between the neuron behavior of the model and analytical calculation in Figure 5.1 shows that the LIF neuron is accurately described by the model.

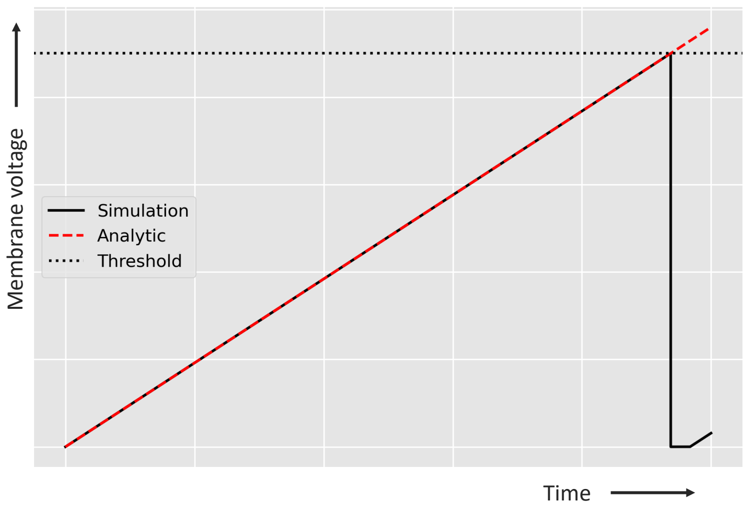

Figure 5.1: The membrane voltage for a single neuron with applied bias current and $\xi = 0$. The analytical solution closely resembles the simulation until the membrane threshold is reached, indicating correct behavior.

5.2.3. Spike Input

To see whether the simulated neuron correctly responds to input stimuli from other neurons, a single neuron receiving a bias current and 5 presynaptic input spikes are simulated. As shown in Figure 5.2, the input spikes inject charge into the postsynaptic neuron. The membrane potential slowly increases to the threshold value but reaches it more quickly than it would without the additional spikes. This agrees well with the behavior of the neurons and synapses on the Innatera prototype.

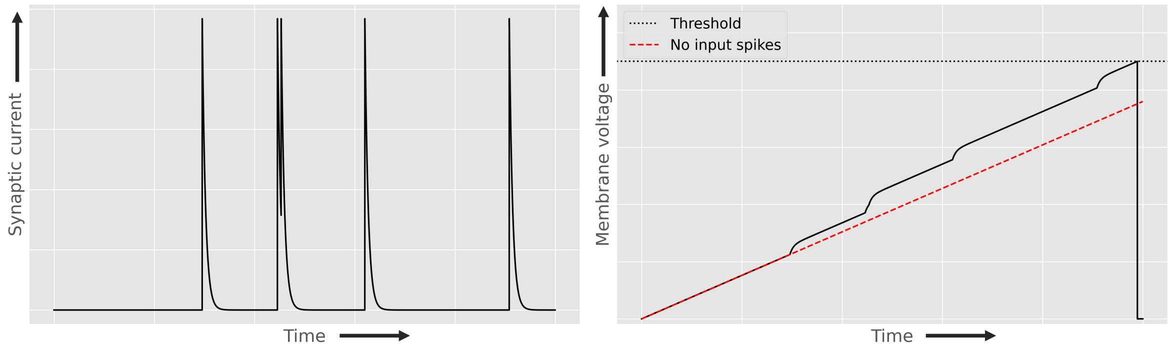

Figure 5.2: The influence of five PSPs (left) on the membrane voltage (right) for a single neuron with applied bias current and $\xi = 0$. The membrane voltage crosses the threshold and produces a spike. The red line indicates the scenario where only a bias current would be applied.

5.3. Model Validation

The validation process is used to test if the simulated network can predict the behavior of the real-world system under various conditions. The purpose of validation is to assess the accuracy and reliability of the simulation model in predicting the behavior of the neurons and synapses on the Innatera prototype. Multiple tests have been conducted to find values for the model parameters described in Table 5.2. These are described in Appendix A.

Parameter	Symbol	Description
Neuron		
Reset voltage	V_r	The voltage to which the neuron membrane drops after firing
Threshold voltage	V_{th}	The threshold that needs to be exceeded by the membrane voltage to cause a neuron to fire
Refractory period	t_{ref}	The period after firing when a neuron does not receive any input
Capacitance	C	The capacitance of a neuron determining the electrical behavior
Noise	ξ	Small high-frequency variations in the membrane voltage of (analog) neurons
Mismatch	m	The structural deviation between electrical parameters of (analog) neurons and synapses
Leakage current	I_{leak}	The leakage current drawing charge from the neuron membrane
Unit bias current	I_{bias0}	A (circuitry) constant that determines the strength of the input bias current to a neuron
Synapse		
Synaptic time constant	τ_{syn}	The time constant that determines the width of a PSP
Unit synaptic amplitude	I_{syn0}	The (circuitry) gain of a synapse that is multiplied by the weight setting to determine the height of a PSP
Synaptic delay	t_{delay}	The delay between the arrival of a presynaptic spike and the generation of a PSP in a synapse

Table 5.2: The model parameters.

5.4. Networks

In the simulation phase, the goal is to determine what networks can be used that enable radiation interactions to be observed and analyzed. To investigate what SNNs could be used for that purpose, a systems engineering approach was adopted using a list of requirements as a starting point (Table 5.3). The selected networks are explained in detail in the following sections.

Label	Requirement
NET-1	The network shall be implementable on the Innatera prototype.
NET-2	The network shall be implementable in Brian2.
NET-3	The network shall have a characteristic operation that is determined by the setting of parameters.
NET-4	The network shall allow reasoning about the input-output correlation without a large level of abstraction.
NET-5	The network shall have an architecture that is easy to understand and modify.
NET-6	The network shall be structured such that the knowledge gained from it can be effectively applied to real-world problems and used to develop practical applications.
NET-7	The network shall minimize any Silent Data Corruption (SDC).

Table 5.3: Network requirements

5.4.1. Intrinsic Stimulation Network

An intrinsic stimulation network is used for its ease of implementation in simulation and its explainability. The network consists of a fully-connected SNN with all synaptic weights set to zero, which results in the behavior of each individual neuron being only dependent on the bias current. All neurons are given an individually calibrated bias to induce spiking at a target firing rate of 100 kHz as shown in Figure 5.3. This results in predictable spiking behavior for each neuron as long as there are no external perturbations. However, if additional noise, synaptic weight changes, or neuron parameter changes are introduced, the spiking behavior of the individual neurons will likely change. In this way, the influence of radiation on an SNN can be measured.

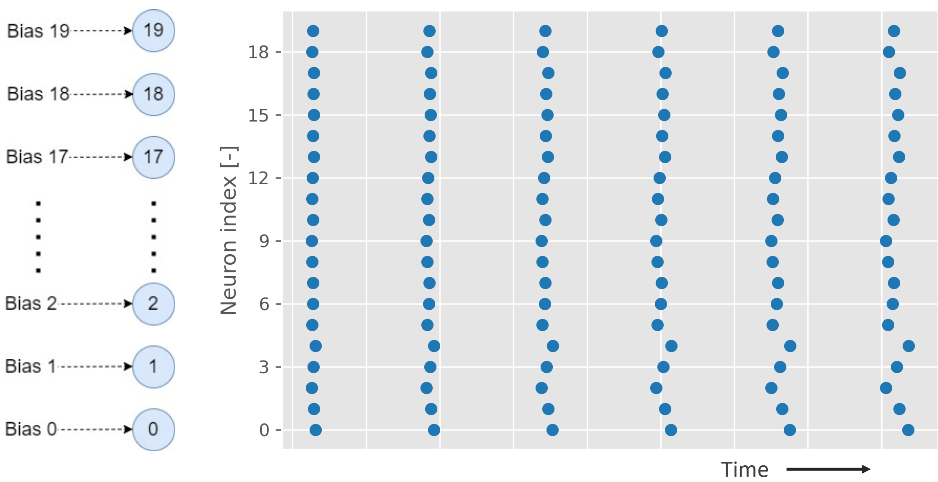

Figure 5.3: A schematic overview of the intrinsic stimulation network with calibrated input bias for each neuron (left). The output spikes for each of the 20 neurons in the network are represented as points over time (right). The neurons are given slightly different parameters that would resemble real analog neurons.

5.4.2. Synfire Chain

To achieve network functionality while maintaining a relatively understandable structure, the synfire chain was selected [80]. It consists of a chain of fully connected groups, also known as *nodes*, containing at least one neuron. The chain is completed by connecting the last receiving node to the first sending node of the chain. This structure and the output spikes for each group are visualized in Figure 5.4.

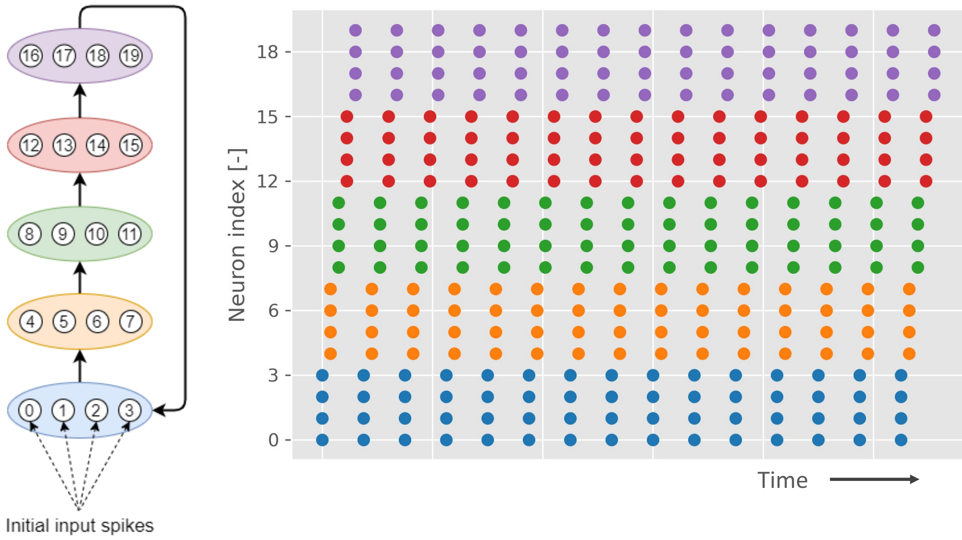

Figure 5.4: Example of a synfire chain consisting of 5 nodes of 4 neurons. The arrows indicate in which way the nodes are fully-connected. The structure represented visually (left) exhibits firing behavior (right) in a predictable manner.

Whenever *n* cells from the sending node become synchronously active, it is expected that at least *k* cells of the receiving node will become synchronously active (where *k* is not smaller than *n*) [80]. So, if all neurons in the first group are activated synchronously, they will cause the neurons of the second group to fire synchronously, and so on. Thus, each activated group will pass a spike volley on to the next group, where the time between the spiking of different groups is dominated by the synaptic delay. This process is visualized in Figure 5.4.

Depending on parameters such as the number of spikes put into the system, their temporal dispersion, synaptic weights between neurons, and the number of neurons in each group, a synfire chain can occupy one of several modes of operation [81, 82]:

1. The spike volley propagates more or less unaffected through the entire chain in a temporally stable manner for as long as it is measured.

2. The network only shows a stimulus-induced increase in activity, after which the activity vanishes.

3. The network only shows precise synfire operation at the start of the operation, after which it will become chaotic and fire constantly.

If the synfire chain achieves stable operation, this process will continue until other processes (e.g., radiation effects) injected from the outside interfere, disturbing the activity propagation [81, 82]. This would therefore allow a relatively straightforward estimation of the level of influence caused by radiation effects during experiments.

5.5. Radiation Model

The goal of creating a radiation model is to be able to simulate complex radiation environments and to explore a wide range of mitigation strategies agnostic of the NC hardware implementation and SNN characteristics. To fully address the requirements the model has to adhere to, Table 5.4 was composed.

Label	Requirement
RM-1	The radiation model shall incorporate Single Event Upset (SEU)s.
RM-2	The radiation model shall incorporate Single Event Transient (SET)s.
RM-3	The radiation model shall incorporate TID.
RM-4	The radiation model shall implementation of combinations of SEUs, SEEs, and TID to different degrees.
RM-5	The radiation model shall be applicable to a wide range of SNNs
RM-6	The radiation model shall be validated using experimental data from the Innatera T0 prototype.
RM-7	The radiation model shall be tunable to allow its application to other NC hardware.
RM-8	The radiation model shall be implementable in Brian2.

Table 5.4: Radiation model requirements

A bottom-up approach was chosen to create a parametric noise model for each component of the network, including synapses and neurons, to incorporate the effects of radiation. The radiation effect models aim to capture the overall impact of radiation on the macroscopic spiking characteristics of neurons. To achieve this, radiation models are proposed based on the theory mentioned in chapter 4, and the parameters are tuned using experimental results.

5.5.1. Total Ionizing Dose

The effects of TID are incorporated in the simulation as a change in the electrical parameters of the circuits on the chip as mentioned in subsection 4.3.1. For the neurons, this includes the capacitance, leakage, and threshold voltage as shown in Equation 4.1. Also, it is expected that the bias current might change as a result of TID. The operation of the synapses could also be affected, especially with regard to changes in the unit synaptic amplitude and synaptic delay. Since the electrical parameters are implemented in the simulation as values, they can be decreased or increased over the course of the simulation to simulate TID effects. The magnitude of this change with respect to the accumulated dose in the Device Under Test (DUT) can be tuned using experimental data as shown in Figure 5.5.

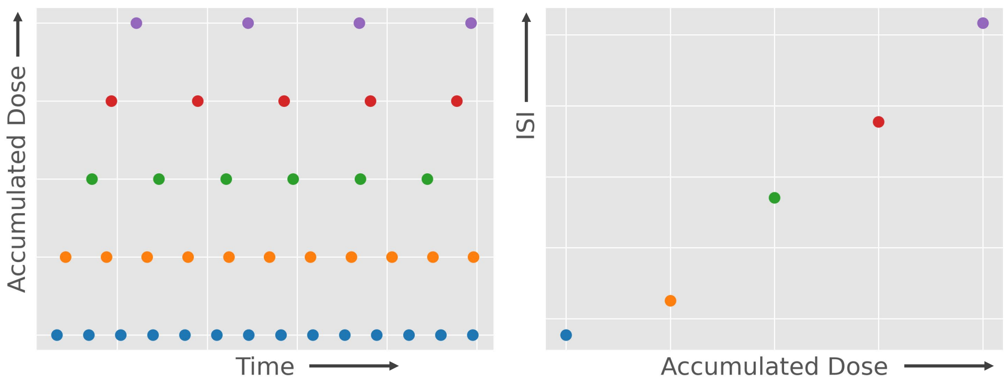

Figure 5.5: The result of TID on the ISI of an ideal neuron during simulation. Several tests are conducted where the electrical parameters of the neuron are gradually decreased. The effects on the spiking behavior over time (left) and the resulting ISI (right) are presented.

5.5.2. Single Event Upsets

The SEUs in the model are introduced as an SEU Induced Parameter Perturbation (SIPP). These SIPPs are spread out over the course of the simulation using a Poisson distribution. The number of injected SEUs can be tuned using the detected number of events for different beam settings. Once the simulation reaches one of these SIPP timestamps, it pauses and replaces one of the parameters of a neuron or synapse with a randomly selected value where the available values closely resemble those utilized in the Innatera prototype. A visualization of a simulated SIPP in a neuron parameter is presented in Figure 5.6.

To estimate which particular SIPPs occur more often than other SIPPs, the number of bits employed for a particular parameter setting is used. It is assumed that parameters that use many bits (e.g. the value of the synaptic weight consisting of multiple bits) are more likely to be changed due to an SEU than parameters that use few bits (e.g. the sign of a synaptic weight consisting of a single bit).

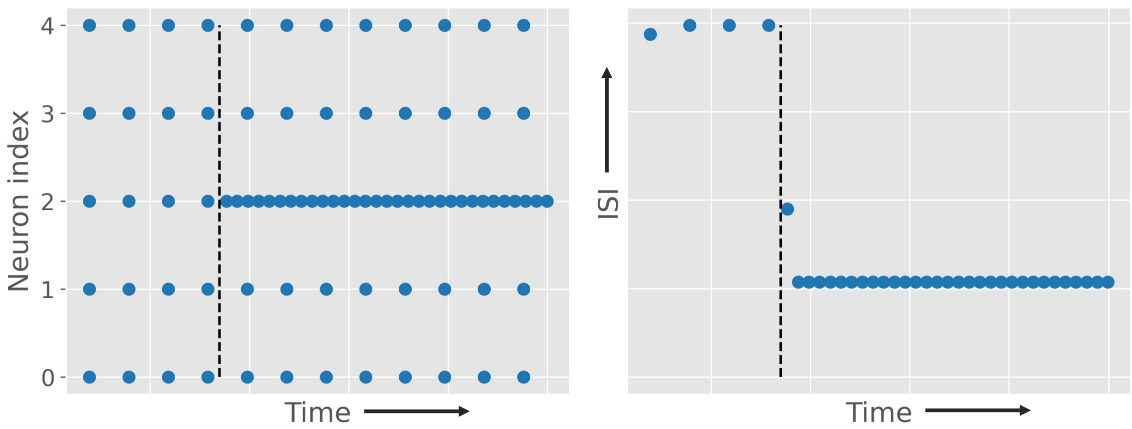

Figure 5.6: The result of an SEU on the ISI of an ideal neuron during simulation. A group of 5 neurons is simulated, and an SEU is injected into neuron 2 at the dashed line

5.5.3. Single Event Transients

The effect of an SET on the electrical behavior of a neuron or synapse is assumed to be mostly dependent on the amount of charge deposited in the sensitive volume and the location in the circuit where the interaction takes place [83]. This process is modeled using a decaying spike in the input current to allow SETs to have an effect over multiple output spikes. SETs are modeled with two parameters to allow changing the height and width of the spike as follows:

$$\frac{di_{SET}}{dt} = -\frac{i_{SET}}{\tau_{SET}} \tag{5.1}$$

Where i_{SET} denotes the height of the current spike and τ_{SET} denotes the time constant that determines the width of the spike. An example of a simulated SET is shown in Figure 5.7. This SET results in the neuron firing at a higher rate. However, by changing the sign, magnitude, and time constant of the SET, practically all electrical behaviors can be modeled.

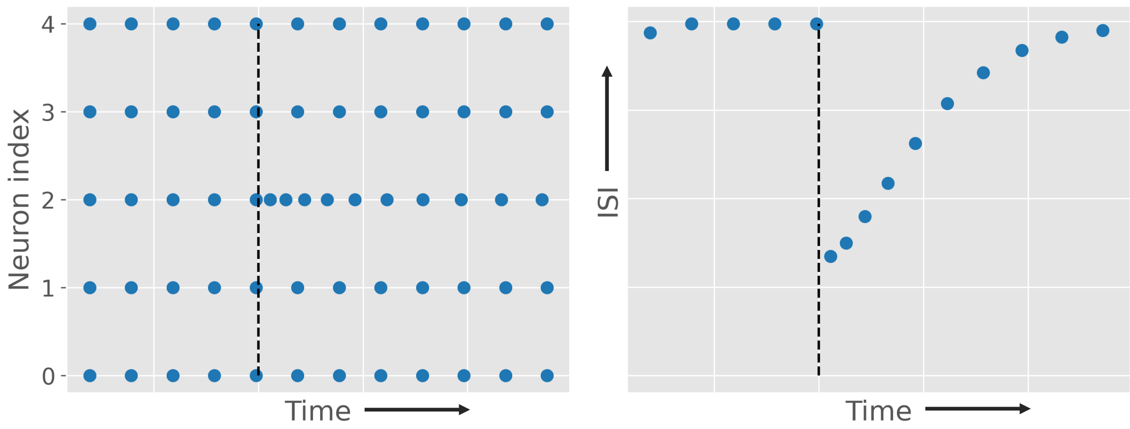

Figure 5.7: The result of an SET on the ISI of an ideal neuron during simulation. A group of 5 neurons is simulated, and an SET is injected into neuron 2 at the dashed line.

5.6. Experimental setup

The test objective is to investigate the effects of SEEs and TID on the digital and analog elements of the T0 prototype. To systematically approach the test procedure, a distinction is made between the system, comprising the neuromorphic processor, peripheral systems, laptops, and measuring software, and the test, referring to the radiation environment, timing, safety, and other non-system parameters. A schematic overview of the experimental setup is provided in Figure 5.8.

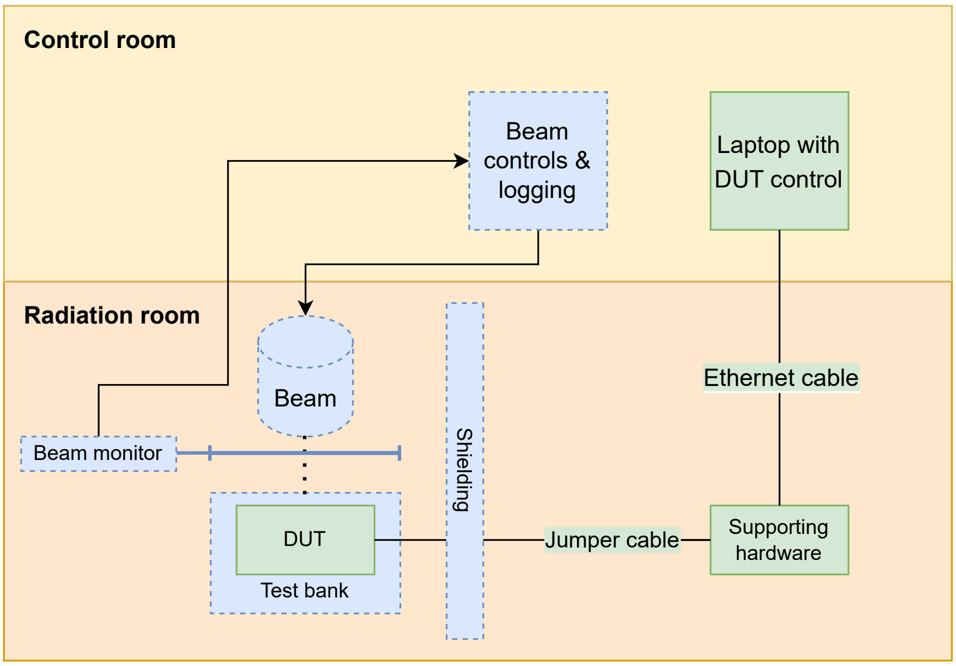

Figure 5.8: The test setup used for the proton experiments. The blue dashed blocks indicate test structures, while the green solid blocks indicate system items.

5.6.1. System Requirements

Guidelines for SEE testing with a proton beam were used to determine the necessary capabilities of the experimental system [84, 85]. These were combined with additional prerequisites to streamline experiments and prevent (human) errors to find the overall list of system requirements presented in Table 5.5.

Label	Requirement
SYS-1	The system shall collect and store all relevant (raw) data.
SYS-2	The system shall allow users to enter and edit data.
SYS-3	The system shall display up-to-date and accurate data in a user-friendly and easy-to-understand format.
SYS-4	The system shall perform calculations accurately and in a timely manner.
SYS-5	The system shall generate reports that can be exported and shared.
SYS-6	The system shall be fully functional and responsive for user input at all times.
SYS-7	The system shall correctly store all data entered into the system with a date and timestamp.
SYS-8	The system shall display clear and helpful error messages to the user.
SYS-9	The system shall be capable of initializing the device and performing basic functionality checks.
SYS-10	The system shall provide dynamic processor operation while under irradiation.
SYS-11	The system shall be capable of resetting/reinitializing the DUT as needed.
SYS-12	The system shall accurately generate a known duty factor (ratio of device sensitive time to total elapsed time).
SYS-13	The system shall conduct post-irradiation tests to verify that the device has not suffered any hard damage.

Table 5.5: System requirements for experimentation.

5.6.2. System Information

The information presented in Table 5.6 gives a brief overview of the system used to perform the experiments.

Item	Description
Device	Innatera T0 prototype
Description	A mixed-signal neuromorphic processor on a development board connected via jumper cable to an Field-Programmable Gate Array (FPGA)
Technology node	28 nm node size
Packaging	Socket
Device preparation	Not necessary
Sample size	2 DUT and 1 control device
Sample selection	Laboratory functionality testing and visual inspection
Peripheral systems	Xilinx Zynq-7000 System-on-Chip (SoC) ZC706 FPGA and two laptops with Excel and Python
Control software	Custom Python scripts (see section 5.4)
Measurement software	Custom Python Graphical User Interface (GUI) and logging scripts

Table 5.6: Information on the device used for experiments.

The Innatera prototype and FPGA were installed in the beamline of the proton beam where lead shielding was used to shield the supporting hardware from radiation exposure as can be observed in Figure 5.9.

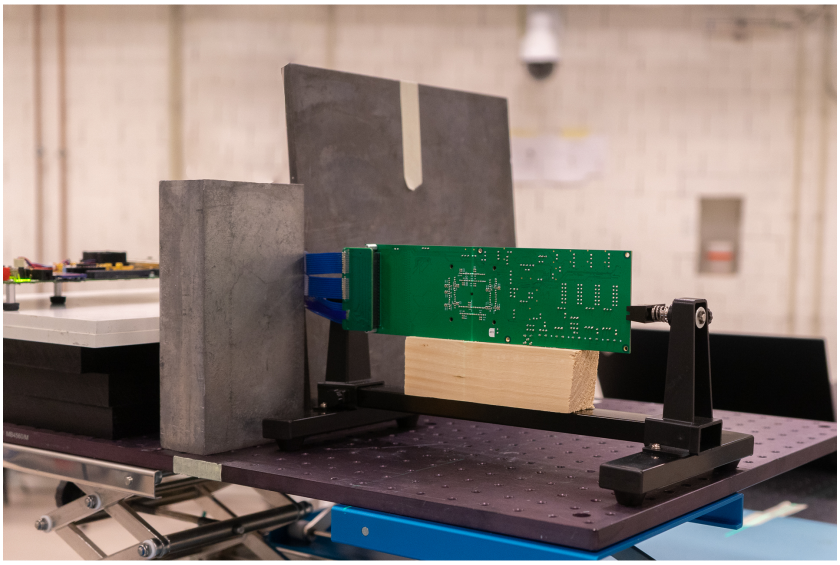

Figure 5.9: The backside of the development board with T0 prototype in the beamline with connections to the FPGA on the other side of the lead shielding.

The Innatera Prototype

Innatera's processors are considered to be suitable for potential space applications because of the standard operating software (PyTorch), low power consumption (due to mixed-signal operation), and focus on smart sensing and edge processing [41, 21]. In this research, a mixed-signal Innatera prototype is used, which combines aspects from analog and digital NC. This prototype is originally intended for rapid prototyping of specific subsections of designated intellectual property within the Innatera portfolio, so it does not represent Innatera's main-line chip offering. However, since it does contain neurons and synapses as described in chapter 4.

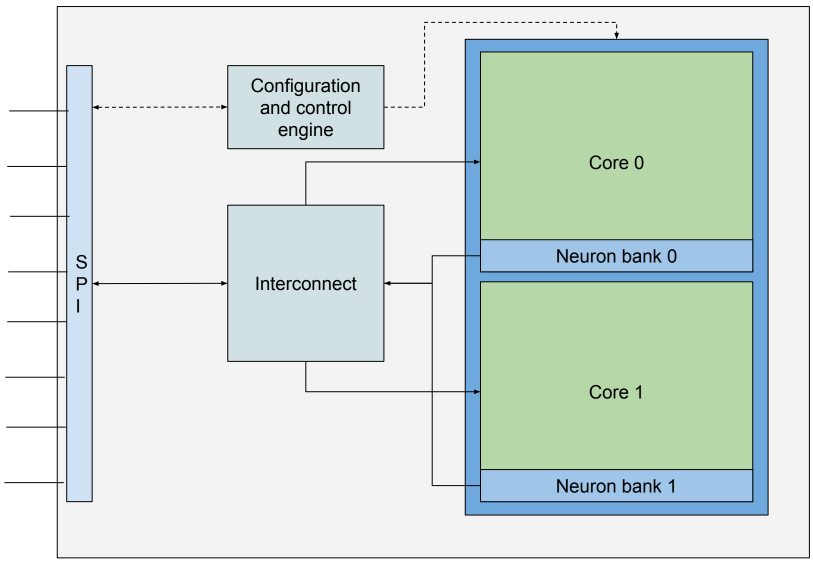

Figure 5.10: A schematic overview of the Innatera T0 prototype.

The processor is an accelerator for SNNs. The mixed-signal array of neurosynaptic segments, shown on the right of Figure 5.10, performs spike integration and generation. The array contains two uncalibrated neurosynaptic segments consisting of analog neurons and synapses. Each of the segments contains a crossbar array of synapses and a number of neurons that are connected through a switch matrix and an interconnect. This allows spikes to travel between the two neuromorphic arrays and the input/output interface. A configuration and control engine is also present for initializing the device and setting parameters.

5.6.3. Test Requirements

Test requirements are a very important aspect of a radiation test campaign. These requirements dictate what the tests must look like in terms of safety, repeatability, planning, and other areas crucial to performing successful tests. The test requirements composed for the radiation experiments in this research are provided in Table 5.7.

Label	Requirement
T-1	The test shall allow different settings for beam energy and fluence.
T-2	The test shall be easily repeatable.
T-3	The test shall expose the system to ionizing radiation in a controlled manner.
T-4	The test shall be safe for all human personnel.
T-5	The test shall be conducted under known environmental conditions, such as temperature and humidity.
T-6	The test shall check for any hard damage to the processor after every exposure.
T-7	The test shall allow switching radiation on and off in a short time frame (< 1 minute).
T-8	The test shall measure the characteristics of the beam during irradiation for reporting purposes.

Table 5.7: Test requirements for experimentation.

5.6.4. Test Information

The proton tests are conducted at the Holland Protonen Therapie Centrum in Delft, a facility that has an agreement with the TU Delft with the aim to cooperate on research in several fields such as nuclear physics, biology, and spaceflight. The facility itself consists of four rooms, of which three are dedicated to patient treatment, and one is dedicated to Research & Development (R&D). The protons are provided by a cyclotron that is connected to all radiation rooms. The proton beam can be directed magnetically to one of the radiation rooms. Electronics and other research objects that do not need the equipment used for patients can be tested in the R&D room, which is equipped with a horizontal, stationary beamline. Unless the beam is operational, entry to this radiation room is permitted, for example, when a power cycle of the DUT is required.

The facility offers a range of fluxes and beam energy levels and provides flux measurements after the test. A beam monitor from HollandPTC is used to measure the proton beam flux, energy, and uniformity. Furthermore, the facility provides the test personnel with multiple cameras pointed at the DUT for visual observation as well as measurements of the temperature and ambient pressure.

Beam Size

The first setting needed for beam calibration is the size. There are three possible settings for the size of the beam at HollandPTC: 100x100 mm, 40x40 mm, and approximately 5x5 mm, also referred to as pencil beam, which is shown in Figure 5.11. Maintaining a constant beam size throughout all tests is preferable since this is inherently difficult and time-consuming to change. Therefore, the choice was made to use the pencil beam throughout all tests to ensure that most radiation impinges only on the DUT without influencing the peripheral systems.

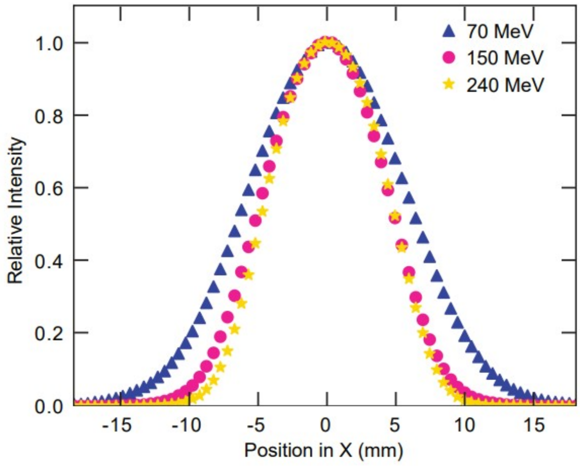

Figure 5.11: The relative intensity of the pencil beam with respect to the position on the detector modeled with a Gaussian [86]. As can be observed, the pencil beam is not precisely 5x5 mm.

Particle Flux

The cyclotron at HollandPTC utilizes an input nominal beam current, which is proportional to the (time-averaged) particle flux. The conversion factors to calculate the flux are determined by calibrating the beam using the beam monitor as follows:

1. Irradiate a detector for a certain amount of time at a certain nominal beam current and particle energy.
2. Measure the total amount of dose received.
3. Convert total dose to fluence using:

$$\phi = \frac{D \cdot \rho}{\frac{dE}{dx} \cdot 1{,}602 \cdot 10^{-19}} \tag{5.2}$$

   Where D is the accumulated dose, ρ is the density of the medium (air), $\frac{dE}{dx}$ is the energy loss per unit distance in the medium at a certain energy level and ϕ is the flux. HollandPTC calculates this energy loss using the method mentioned by Newhauser and Zhang [87]. For calculating deposited dose in another material than air, the ratio between the stopping power of the two materials can be used.
4. Convert the fluence using the surface area of the detector to find the fluence over the area.
5. Calculate the time-averaged flux using the duration of irradiation.
6. Repeat this process for several beam current settings.
7. The relation between the nominal beam current and the flux at the target is now determined. This relationship is linear, so interpolating between the known points gives the flux at the target for all possible beam settings.

Unfortunately, the actual beam current fluctuates by about 30 % around the nominal beam current setting. Therefore, the counts produced by the beam monitor are used to correct this during the data analysis. The dose at the target is proportional to the number of counts in the beam monitor. The received dose is also linearly proportional to the flux. Therefore one can write:

$$\begin{aligned} D &= \alpha \cdot N \\ D &= \beta \cdot \Phi \end{aligned} \tag{5.3}$$

Where D is the dose, α and β are constants, N is the number of counts reported by the beam monitor, and ϕ is the total proton fluence. This can then be rewritten to:

$$N \cdot \left(\frac{\alpha}{\beta}\right) = \Phi \tag{5.4}$$

This allows easy calculation of the actual fluence or flux using the measured number of counts from the beam monitor to ensure accurate dosimetry. The values for α and β can be determined using the process mentioned at the start of this paragraph.
For proton SEE testing, guidelines mention using a maximum flux of 1E10cm^{-2}s^{-1} to 1E11cm^{-2}s^{-1} in order to obtain statistically significant results [84, 85]. However, higher fluxes may be acceptable if can be demonstrated that the test results are not invalidated by other effects, such as device heating, charge collection effects, or tester limits.

Particle Energy

The particle energy is another important beam parameter that is set by the beam operator. The energy of the particles provided by the cyclotron is 240 MeV which can be slowed down to 70 MeV or a desired energy level between these values. This is done by placing degraders in the beam path. The use of degraders presents an issue known as *straggle*, referring to the energy spread around the average energy of a proton beam after passing through a certain thickness of the degrader material. The energy loss is probabilistic, causing the spread to increase with thicker degraders. This spread can also be observed in the size of the beam for different energy levels as shown in Figure 5.11 although scattering as a result of the beam passing through the air in the R&D room also contributes [86]. Straggle can be disregarded at low degrader thicknesses that only slightly reduce energy. However, if thick degraders are employed to significantly lower the average beam energy, straggle can introduce errors in the analysis of the SEE sensitivity of the DUT [84]. For this research, the entire available energy range of 70 MeV to 244 MeV was used without correcting for straggle since the average induced change in beam energy is less than 1% [86]. Also, the proton penetration depth in the irradiated material is sufficient over the entire energy range to reach the sensitive region of the DUT [88].

Test Description

At the facility, Electrostatic Discharge (ESD) protection and DUT fixtures are placed on the beam platform. A jumper cable is connected between the development board and FPGA, which has a power supply and Ethernet cable connected to it. Via an Ethernet switch, the connection is established to the laptop in the control room. Lead shielding is arranged for the FPGA, and connectivity is checked by running characterization and mock tests.

Consequently, energy and flux levels for each particular test are confirmed with the operator and recorded in a spreadsheet. Proton beam testing is then carried out, while real-time statistics are checked using a GUI in the control room. Using these observations, the preliminary level of radiation interactions can be estimated to guide the experimental process.

After testing, all test data is backed up to a secure cloud environment, and raw beam data is obtained from HollandPTC. Materials are collected from HollandPTC in the following days, depending on the level of radioactivity in the irradiated materials.
With this standard procedure that remained unchanged throughout the test campaign, two different types of tests were conducted.

Test 1 - Characterization

The first test is aimed at characterizing the effects caused by radiation using an intrinsic stimulation network (as proposed in subsection 5.4.1). In the characterization test, the following hypotheses are proposed:

- Lasting changes to the firing rate of individual neurons might occur due to SEUs.
- Momentary changes to the firing rate of individual neurons might occur due to SETs.
- Parameters with more bits may be influenced by SIPPs more often.
- SETs might not be measurable by the system due to the stochasticity of the analog components
- TID may increase or decrease the firing rate of all neurons on the chip
- Errors may propagate to the peripheral systems necessitating a power cycle.

During the test, the intrinsic stimulation runs on the DUT before, during, and after exposure to radiation. To detect SEE effects, the spike times are measured for each neuron and the average Inter-Spike Interval (ISI) for each neuron is displayed in the GUI. This allows inference of the occurrence of SEEs in real-time. After irradiation, individual neurons are biased to determine whether synaptic weights have been altered. If other neurons also spike, this is an indication of synaptic weight updates. The result of this process is shown in Figure 5.12. The system is then reset to restore all parameter changes due to SIPPs for the next test iteration.

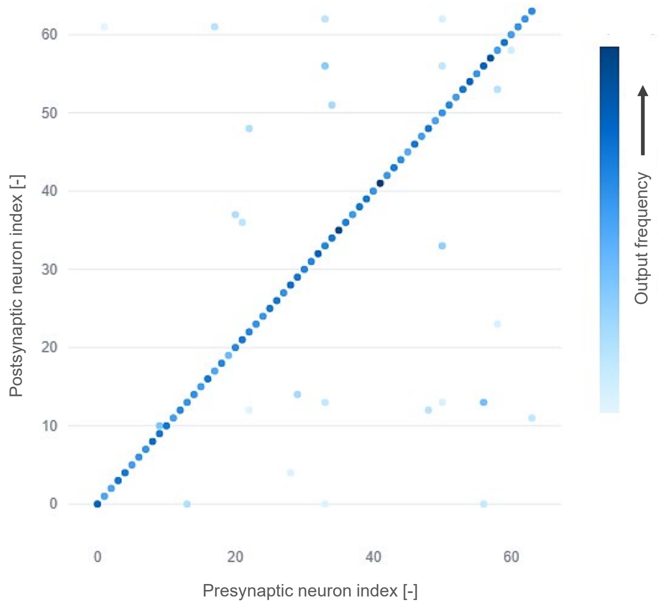

Figure 5.12: A simulated example of what the output would look like if a number of synapses were subjected to SIPPs setting excitatory weights. The diagonal data points indicate that a neuron spikes if it is stimulated. The other data points indicate that a postsynaptic neuron fires if another presynaptic neuron is stimulated.

Network Operation

The second test aims at analyzing the operation of a synfire chain network under irradiation (as mentioned in subsection 5.4.2). In the network operation test, the following hypotheses are proposed:

- The gradual buildup of SEUs may have a strong effect on the network operation.
- The short-lived disruption caused by SETs may have a weak effect on the network operation.
- The network operation under radiation may be affected differently for synfire chain networks with different connectivity.
- The network operation under radiation may be affected differently for synfire chain networks with different synaptic weights.

The test aims to determine the effects of SEEs and TID on the network performance and how the network responds to these perturbations. The synfire chain's correct operation is expected to be disrupted by radiation effects as mentioned in subsection 5.4.2. Three potential sources could cause instability: temporal dispersion of the spike packet, spontaneous activity, or connectivity perturbation. These factors can be influenced by SEUs, SETs, and TID. Therefore, the synfire operation is analyzed as an abstract measure of the influence of a combination of all radiation effects.

5.7. Data Analysis

There are two methods to observe neurons on the chip: high-resolution observation of a single pair of neurons with a high temporal resolution or observation of all neurons with a resolution that is ~2000

times lower. In the low-resolution method, spikes from individual neurons are grouped within a timestamp, potentially causing multiple spikes to be counted as a single spike at a high output frequency. This is similar to sampling a signal below the Nyquist frequency. Additionally, variations in spiking frequency over time due to the analog nature of neurons may not be reflected in the output. The standard deviation of the ISI within correct subsequent time bins would approach zero, complicating the analysis of outliers.
To see how radiation would influence the spiking of neurons, the research was split into several different individual inspections. First, the calibration data was used to investigate whether or not the chip suffered from TID effects over the course of multiple exposures. Secondly, the data of each test was inspected individually to detect SEEs.

5.7.1. TID Detection

As demonstrated, the spiking characteristics of an individual neuron in a mixed-signal neuromorphic circuit can be influenced by many factors, both digital and analog. It was assumed that the most important TID effects would be long-lived and build up inside the device over several exposures, as shown in Figure 5.5. These effects should therefore be more pronounced after every radiation test run. This could eventually lead to failure but also allows any related effects to be analyzed separately from other analog or digital effects.

To find the drift for each individual neuron, a bias sweep over all possible current settings was performed before each test run for each individual neuron. By comparing these values over several experiments, it can be determined whether the spiking rate of neurons is influenced by TID effects accumulating in the chip. Using a calibrated beam dose rate, the amount of TID-induced drift of the ISI per neuron as well as the spread of ISI per bias current level, can be calculated.

5.7.2. SEU Detection

Data corruptions resulting from SEUs are assumed to be long-lived (e.g. > 1 ms) because a flipped bit will likely remain that way, and the chances of that particular bit being struck again and flipping back are considered to be small. Because of the longevity of the digital effects, a moving average can be used along with a moving standard deviation to obtain a more stable representation of the actual spiking frequency per neuron. To determine the optimal window size for the moving average, a set of indicators was employed:

- The number of detected SEUs occurring before and after irradiation should be near zero.
- Visual inspection of the ISI of a sample of detected SEUs should show a sudden change in the neuron's ISI.
- Positive correlation between the number of detected SEUs and particle fluence. However, the occurrence of SEEs is not linearly correlated to the received particle fluence due to other external factors and secondary effects such as saturation [85].

The rolling average with the best results uses a window of 1 ms. The changes in spiking frequency are found by comparing the rolling average over the next millisecond with the one at the current timestamp. If the average spiking frequency at $t + 1$ ms is not within three standard deviations from the average spiking frequency at t, it is marked as an SEU.

SEU Types

To gain some insight into where the NC prototype is most vulnerable to SEUs, a secondary check was performed after every test. Although the SIPPs could occur in a number of different parameters causing the neurons to change their spike output, the effort was made to make a distinction between the susceptible parameters by overwriting the prototype settings in a fixed order. Consequently, the following distinction can be made:

- Parametric: The change in spiking frequency caused by an SEU persists in the secondary check.
- Bias increase: The spiking frequency increases as a result of an SEU and decreases again during the secondary check (and no excitatory synapse connection is found)

- Inhibitory synaptic weight / Bias decrease: The spiking frequency decreases as a result of an SEU and increases back to the nominal value during the secondary check.
- Excitatory synaptic weight: Biasing a neuron results in spiking in another neuron.
- Unknown: The ISI does not adhere to any of the above.

5.7.3. SET Detection

The transient effects occurring in the device are the most difficult to find and characterize. These effects are generally very short-lived and are assumed to dissipate anywhere between a few nanoseconds and a few microseconds [83]. For each run, all neurons are observed iteratively using the high-resolution observation mode. To detect SETs, rolling averages were composed, each with a different window size. A larger window of 1 millisecond was used to represent the slow gradual changes in ISI that might be caused by a SIPP. A smaller window represents the very sudden changes to the ISI that may be caused by an SET as displayed in Figure 5.7. By comparing these two values over the course of the experiment, outliers can be found. To find the optimal size for the small window, the same sort of indicators as used for detecting SEUs were applied.

5.7.4. Network Operation

As mentioned in subsection 5.4.2, the destabilization of a synfire chain can be used as a measure of the number of perturbations introduced in an SNN. To determine the stability of the synfire operation, the following indicators, visualized in Figure 5.13, were used:

- The level of activity α, is defined as the number of spikes measured at the exact same timestamp within one group.
- The synfire cycle time t_c, is defined as the time between subsequent firing of the same group.
- The synfire causality c, defined as the difference between group numbers that spike directly after one another (e.g. in a perfect synfire chain, group 3 fires after group 2, which fires after group 1, resulting in an average causality of 1). If the difference is smaller than 0, indicating non-causality, the value is multiplied by 2.

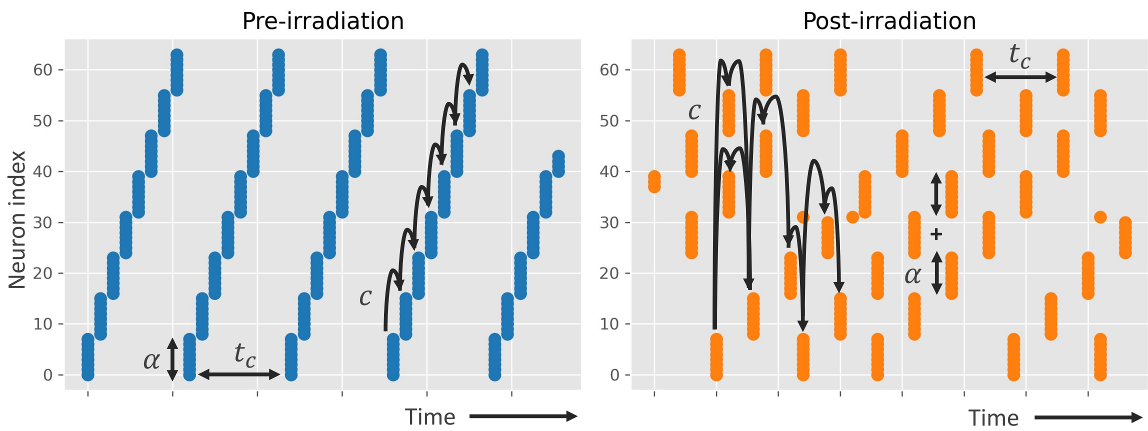

Figure 5.13: The activity α, cycle time t_c, and causality c are calculated for each group and averaged to check the synfire operation. These indicators are drawn into the plot to show how they indicate incorrect behavior. In this example, with a group size of 8 neurons and 8 groups, t_c differs before and after irradiation. Also, several groups fire at the same time after irradiation leading to activation of roughly 167%, while pre-irradiation has perfect 100% activation. Finally, the causality c is 1 before irradiation, while the causality after irradiation is highly distorted ($c = -10$).

To gain some more insight into the relevant parameters of the synfire chain and the susceptibility of the network, multiple sets of slightly different networks were used in the experiments. The two parameters that were investigated were the number of neurons per group and the synaptic weight between each neuron. The number of neurons per group ranged from 4 to 16. For the synaptic weight, making increments between all available values would be inefficient and time-consuming. Therefore, three increments were chosen:

- Operation on the upper limit of stability with strong synaptic weights. This type of network would be prone to destabilize into a chaotic mode of operation.
- Operation in the center of stability with medium synaptic weights. This type of network could potentially destabilize into any mode but was assumed to be the most stable to perturbation.
- Operation on the lower limit of stability, or at *criticality*, with weak synaptic weights. This type of network would be prone to destabilize into a silent/dead mode of operation.

5.8. Mitigation

For mitigating the effects of radiation on a certain network, solutions were considered that adhered to the requirements presented in Table 5.8.

Label	Requirement
MIT-1	The mitigation method shall be implementable in Brian2.
MIT-2	The mitigation method shall be implementable in (new) NC hardware.
MIT-3	The mitigation method shall be applicable to a multitude of SNNs.
MIT-4	The mitigation method shall be implementable without severely degrading SNN speed.
MIT-5	The mitigation method shall be implementable without severely degrading SNN accuracy.

Table 5.8: Mitigation requirements.

A distinction is made between online and offline mitigation measures. Online mitigation includes algorithm changes that enable radiation effects to be mitigated during processing. In contrast, offline methods provide the end user with the capability to appropriately reset the network if there has been a significant decline in performance.

Label	Type	Change in network
GR	Online	Increase group size
NG	Online	Increase number of groups
M	Online	Employ multiple synapses
SW	Online	Increase synaptic weight (through training)
TMR	Offline	Apply Triple Modular Redundancy (TMR)
RS	Offline	Reset network parameters at a fixed rate

Table 5.9: The mitigation strategies applied to the simulated synfire chain.

5.8.1. Online Methods

The online mitigation techniques encompass algorithm changes that can be applied to any SNN to make it more resilient to the effects of radiation during operation. The methods considered here must meet the requirements posed in Table 5.8. Therefore, the main characteristics of these mitigation strategies revolve around simplicity, network independence, and limited hardware demands. The parameter changes necessary for the mitigation methods are described in the following sections where SNN parameters that are not mentioned remain equal to that of the baseline synfire chain.

Synaptic Weights

It is thought that larger synaptic weights tend to help maintain the initial activity level of a synfire chain while exposed to radiation. The effects resulting from SIPPs and SETs are assumed to be lessened relative to the standard operation if stronger synaptic weights are used. Therefore, this effect was investigated to achieve a more reliable network. The synaptic weights for all connections in the synfire chain are increased up to 200 % of the baseline value.

Group Size

It is thought that larger numbers of neurons per group in a synfire chain increase its ability to maintain its initial activity level while being exposed to radiation due to redundancy. In a simulation, it is possible to increase the number of neurons per group to see how this affects the radiation hardness of a synfire chain. Although hardware limitations must be considered, this allows switching group sizes from 1 to virtually any number of neurons. For the mitigation exploration, the group size was increased up to 200 % of the baseline value.

Number of Groups

It is thought that including more groups in a synfire chain increases its ability to maintain its initial activity level while being exposed to radiation due to redundancy. In a simulation, it is possible to increase the number of groups to see how this affects the radiation hardness of a synfire chain. Although hardware limitations must be considered, this allows changing the synfire chain length from 2 to virtually any number of groups. For the mitigation exploration, the number of groups was increased up to 200 % of the baseline value.

Redundant Synapses

If the number of synapses is larger than 1, the synaptic connection will form a multapse connection. If these multapses are tuned such that the summed weight of each link adds up to the same weight as the single synaptic connection, the network performance shall be identical. This is true for practically all SNNs. However, it is thought that having redundant synapses helps to maintain the network operation stable in the case of synaptic SIPPs. For the mitigation exploration, the number of synapses between each neuron was increased up to 800 % of the baseline value.

5.8.2. Offline Methods

For the offline methods, general radiation mitigation measures can be applied. These include software and hardware redundancy (e.g. TMR or RHBD techniques). Since these are fairly well documented and more refined versions exist, these topics are not handled in detail.

Triple Modular Redundancy

TMR is applied to investigate if existing radiation mitigation measures could improve the fault-tolerance of SNNs on NC processors. Copies are made of the initial neuron and synapse parameters that can be influenced by SIPPs during the simulation to emulate TMR. These copies are affected by SIPPs in a similar manner as in the baseline synfire chain model. The network uses the parameters that result from voting between the three individual parameter copies.

Parameter Resetting

Another method to counter SEUs is implementing ECC on the (satellite) onboard computer. This does not necessitate additional hardware but generally increases system run time. One well-known example is Hamming code which allows the system to find SEUs and Multiple Bit Upset (MBU)s [89]. System resets may consequently be performed to reinitialize the corrupted memory elements. To investigate whether this approach would be beneficial for network operation, all parameters of the synfire chain are re-initialized at a fixed rate of 10 Hz.

6

Results and Analysis

In this chapter, the results of the simulations and experimental verification are presented. The data is analyzed, and the impact of radiation effects on the performance of mixed-signal NC processors is discussed. Finally, the effectiveness of the employed mitigation techniques is described.

6.1. Radiation Effect Characterization

The experimental detection and analysis of radiation effects in the Innatera processor are deemed too sensitive to share in the public version of this report. The results are described in Appendix B.

Overall results indicate that:

- The limited parametric degradation of the electrical behavior of the prototype after exposure to $\sim$ 200 krad(Si) indicates that it is highly resistant to TID. The total used dose exceeds radiation levels in most Low Earth Orbit (LEO) satellite applications [90] and those used for testing state-of-the-art (COTS) architectures used in space [91, 92].

- SEUs occur in different digital parameters (mostly in synaptic weights), disrupting network operation over time. By re-initializing the system between tests, these errors disappear.

- SETs are discernible but difficult to detect due to stochasticity in neuron output.

- For a proton (> 70 MeV) fluence that can be found in orbit of less than $\sim 10^8$ particles/cm^2, no SEEs could be detected [93, 94]. This could suggest that the system shows resistance to SEEs; however, accurately estimating the error rate of SEEs for space applications is challenging.

6.1.1. Group Size

The following figures show the effect of different group sizes on the synfire chain operation under irradiation. All the networks presented here are tuned to be operating at the lower limit of stability as mentioned in subsection 5.7.4. In Figure 6.1, it can be observed that the total particle fluence has an influence on the operation of the network, causing destabilization at $\sim 10^{10}$ protons/cm^2. However, the synfire chains destabilize at a different particle fluence depending on the group size. This agrees well with the expected behavior mentioned in section 5.8.

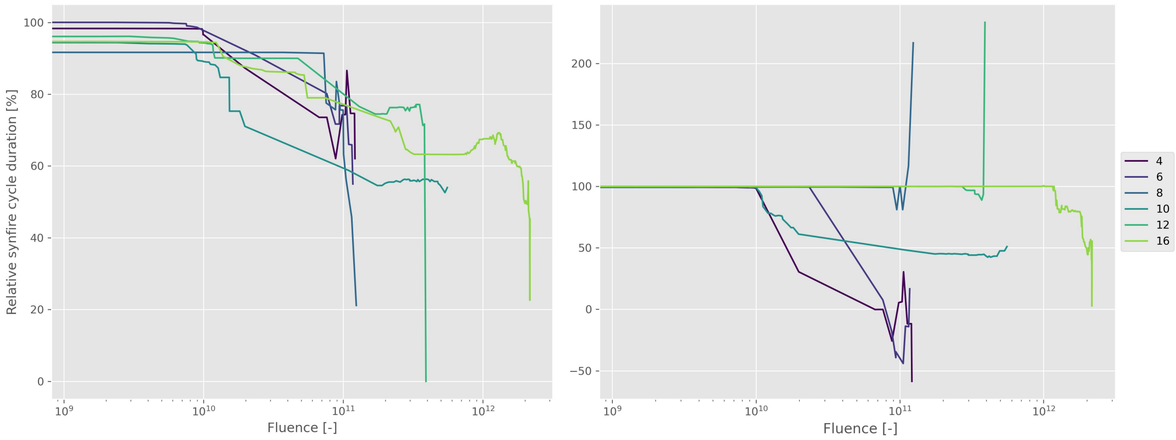

Figure 6.1: The relative cycle duration of several synfire chain experiments with different group sizes. Measurements are composed of multiple tests using beam energy ranging from 70 MeV to 200 MeV and flux ranging from 10^6 to 10^{10} protons/cm²/s.

6.1.2. Synaptic Weights

Networks with stronger synaptic weights stabilize less quickly under the influence of radiation, as demonstrated in Figure 6.2. However, if too large weights are selected, the synfire chain does not achieve stable operation as described in subsection 5.4.2. This is, therefore, not necessarily a good strategy to obtain a stable network.

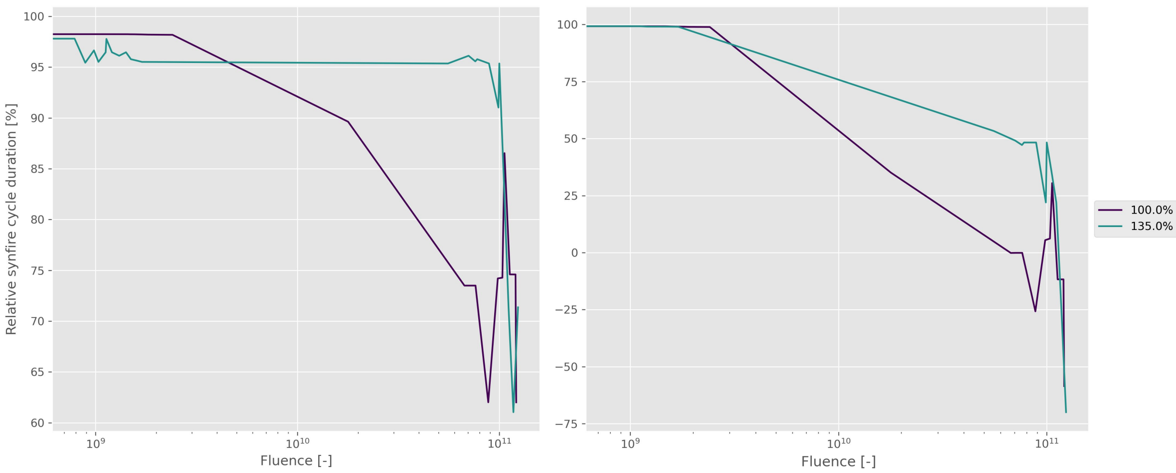

Figure 6.2: The relative cycle duration of several synfire chain experiments with two different synaptic weights. Measurements are composed of multiple tests using beam energy ranging from 70 MeV to 200 MeV and flux ranging from 10^6 to 10^{10} protons/cm²/s.

6.2. Mitigation Results

The simulation results are presented here, where errors are injected into a simulated synfire chain (consisting of 8 groups of 8 neurons) with and without mitigation strategies applied. Only errors due to SEEs are injected without any simulated TID effects since non-linear behavior was measured which is likely hardware dependent. Also, the measured TID effects are small, especially when considered over the course of a single exposure. For the sake of brevity, only plots regarding the synfire cycle time t_c and causality c are displayed, as these provide the clearest distinction between stable and destabilized operations. Overall results are summarized in Table 6.1. The error injection rate is an estimated comparative ratio relative to the baseline network without mitigation applied, showing how many more errors need to be injected for the same loss in network performance. It is important to note that the SEE injection rate is equal for all simulations, while in real-life applications, additional hardware might make the system more vulnerable to SEEs, leading to higher error rates.

Mitigation Method	Error injection factor [-]
None	1
GS	3.2
NG	1.3
SW	2.5
M	2.3
TMR	2.1
RS*	-

Table 6.1: A comparison between the best-performing mitigation methods with respect to the number of errors that can be injected before network operation is severely affected. *Only one simulation destabilized, which indicates that destabilization is still possible but does not occur frequently enough to estimate an error injection factor.

6.2.1. Group Size

As in the experimental results presented in Figure 6.1, the simulation results presented in Figure 6.3 also indicate that larger group sizes increase the stability of the network operation. However, there is no distinguishable correlation between group size and network stability.

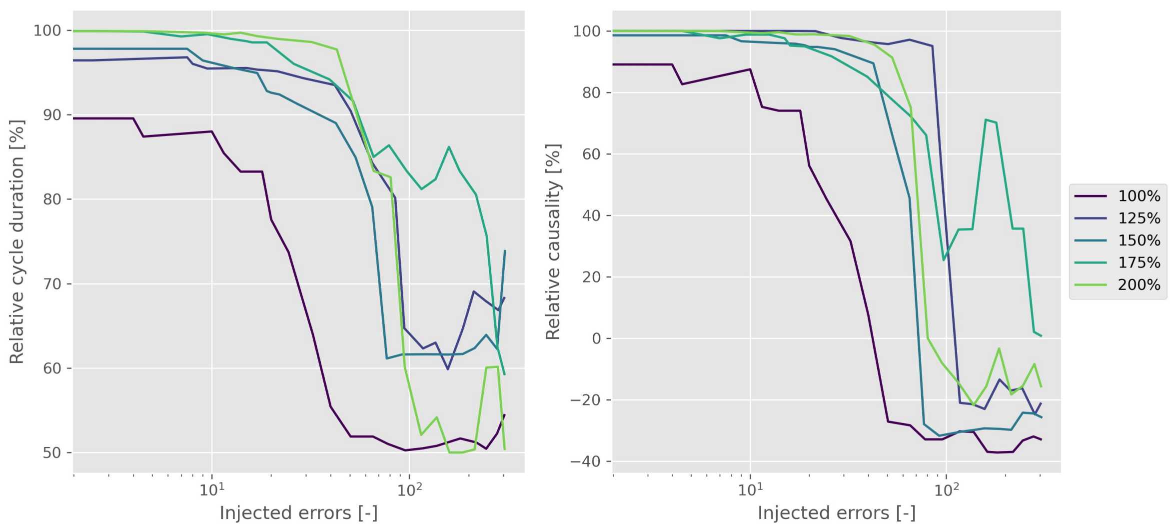

Figure 6.3: The relative cycle duration (left) and causality (right) of several synfire chain trials with different group sizes. These values are indicated relative to the baseline group size of 8 neurons. The displayed graphs are averages composed of 5 simulation trials.

6.2.2. Number of Groups

In Figure 6.4, it can be seen that adding neurons to an existing network does not necessarily increase its fault tolerance. All synfire chains with identical group sizes, irrespective of the number of groups, destabilize at approximately the same number of injected errors.

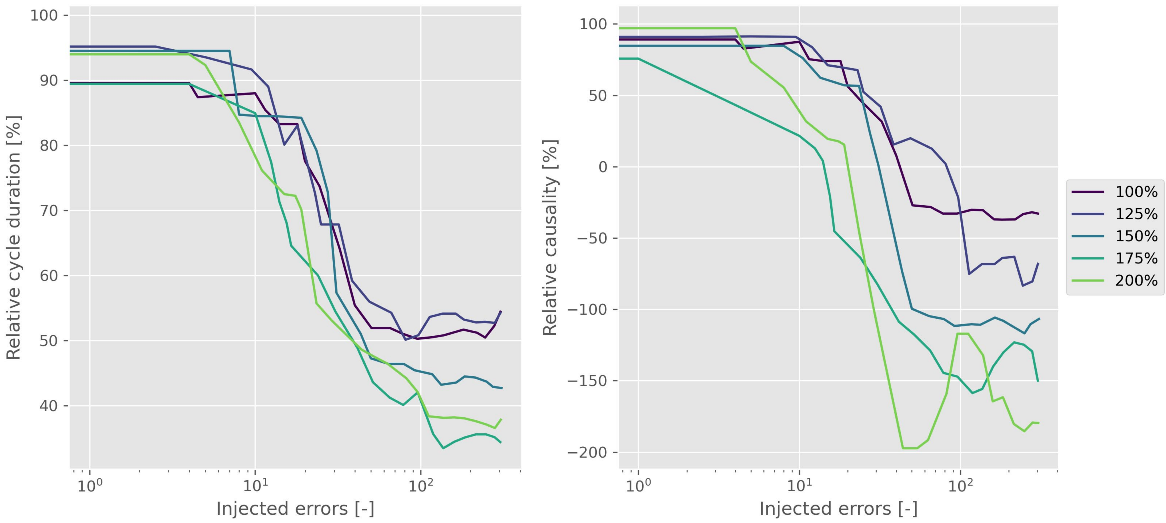

Figure 6.4: The relative cycle duration (left) and causality (right) of several synfire chain trials with 8, 10, 12, 14, or 16 groups. These values are indicated relative to the baseline scenario of 8 groups. The displayed graphs are averages composed of 5 simulation trials.

6.2.3. Synaptic Weights

In Figure 6.5, the destabilization is shown for synaptic weights ranging from 100% to 200% of the baseline scenario. There seems to be an increase in the stability of the operation as the number of injected errors before destabilization differs significantly between the baseline with and without mitigation applied. However, it is clear that this is no straightforward relationship where a stronger weight equals a more stable network.

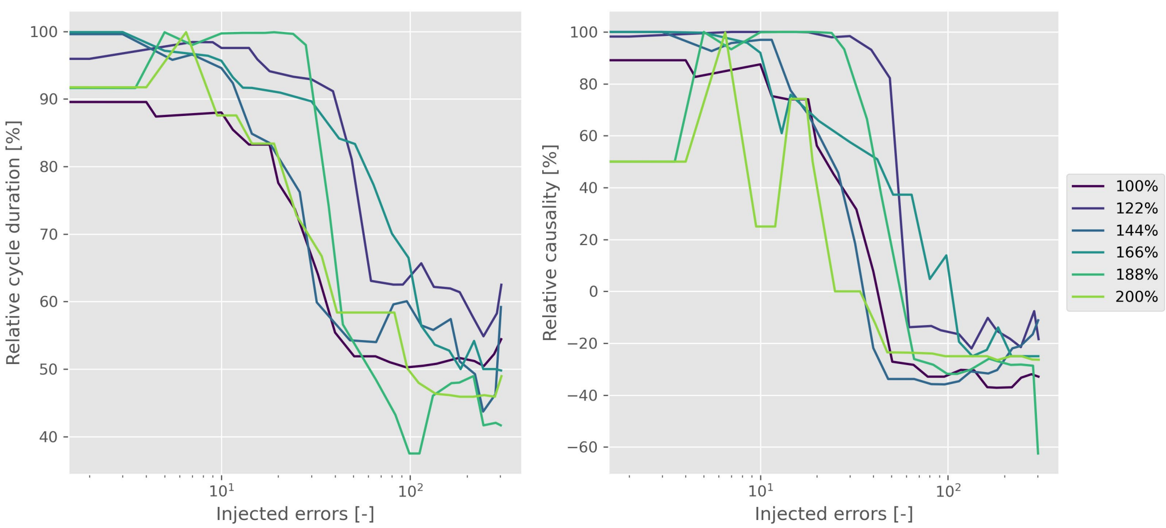

Figure 6.5: The relative cycle duration (left) and causality (right) of several synfire chain trials with different synaptic weights represented as values relative to the baseline scenario. The displayed graphs are averages composed of 5 simulation trials.

6.2.4. Redundant Synapses

In Figure 6.6, it can be seen that including multiple redundant synapses in the network increases its fault tolerance, especially when considering the causality indicator. More detailed analysis also suggests that there is a clear correlation between increasing synapses and network stability.

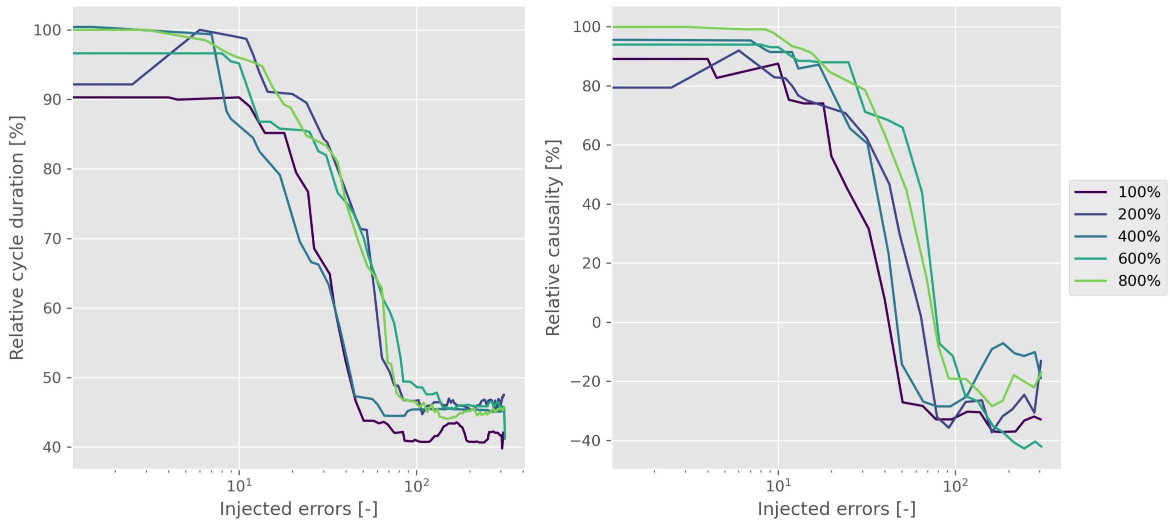

Figure 6.6: The relative cycle duration (left) and causality (right) of several synfire chain trials with different numbers of synapses represented as values relative to the baseline scenario of 1 synapse. The displayed graphs are averages composed of 5 simulation trials.

6.2.5. Triple Modular Redundancy

To see how a conventional method for increasing fault tolerance might influence network stability, one can consider Figure 6.7. Applying TMR clearly increases the network stability. However, it can also be seen that this is not a suitable solution if large numbers of errors are injected.

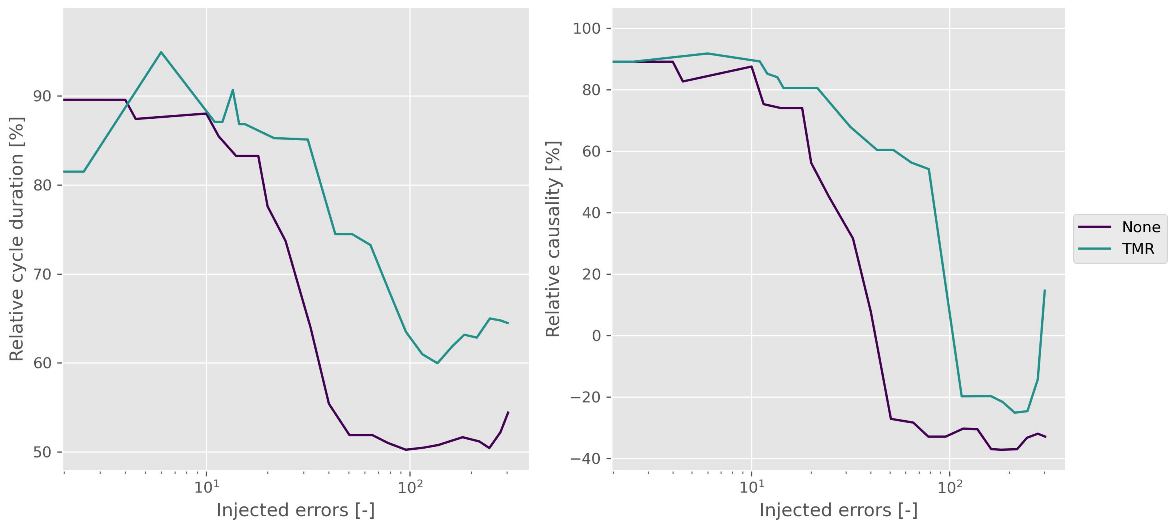

Figure 6.7: The relative cycle duration (left) and causality (right) of several synfire chain trials with and without TMR applied. The displayed graphs are averages composed of 5 simulation trials.

6.2.6. Parameter Resetting

To see how a conventional method for increasing fault tolerance might influence network stability, one can consider Figure 6.8. Re-initializing all parameters once per second clearly increases the network stability. This rate of parameter resetting could be tuned with respect to the frequency of SEE occurrences.

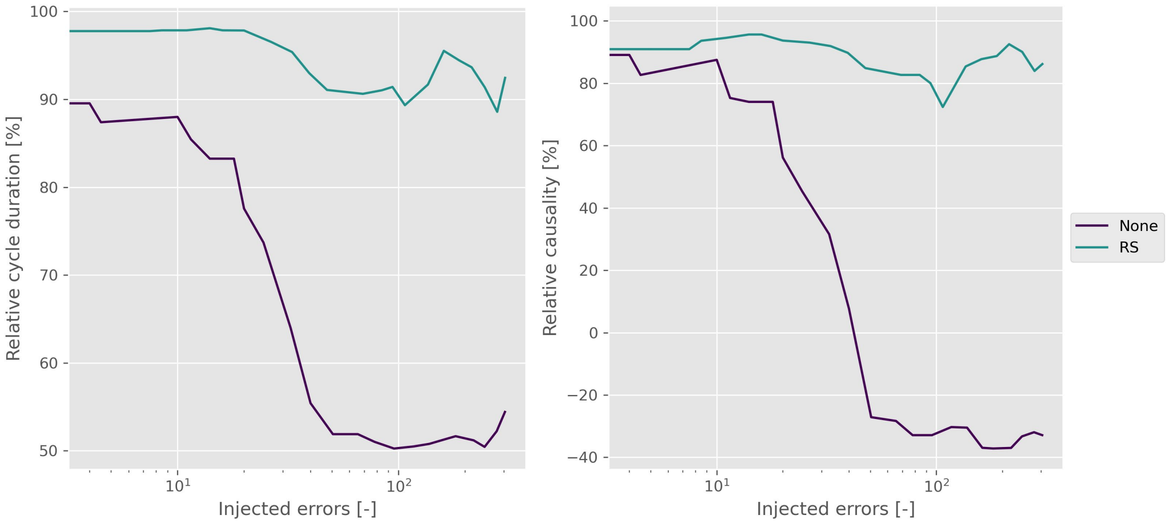

Figure 6.8: The relative cycle duration (left) and causality (right) of several synfire chain trials with and without resetting (indicated as *RS*) of parameters applied. The displayed graphs are averages composed of 5 simulation trials.

7 Discussion

The limitations of the project are discussed along with the implications this has for the results presented in chapter 6. Additionally, the potential directions for research on the effects of radiation on mixed-signal NC are highlighted and recommendations are provided for future researchers based on insights gained.

7.1. Remarks and Constraints

Conducting radiation experiments is a complicated process that requires many different aspects to be taken into account correctly. Unfortunately, the experiments were not set up in the most ideal manner. Firstly, due to the proton energy limitations of the (pencil) beam at HollandPTC, the necessary low-energy measurements could not be obtained to adequately model the relationship between SEEs and particle energy. This rendered the calculation of expected SEE rates for a certain orbit or space application unattainable.

Secondly, the beam limitations also have an impact on the validity of the found TID tolerance. Generally, lower doserates are used for these explorations to better emulate the low-dose environment in space. However, to combine the SEE and TID research, the choice was made to use high calibrated doserates but this is not an ideal scenario. The doserates are calculated for the size of a pencil beam. Despite the packaged prototype being larger than the beam, the actual size of the silicon chip is slightly smaller. The beam doserates have not been adjusted to consider this, potentially leading to an overestimation of the reported dose rate and flux that actually affected the DUT. Considering the relatively high doserates used, the reported tolerance to TID may be overly optimistic compared to actual scenarios in space applications.

Third, there are many parameters that could influence how a specific particle interaction could impact the operation of an SNN on the chip. In this research, the experimental setup only allowed for indirect observation of radiation effects. It is possible that SIPPs would not be noticeable in the used DUT output. This could be due to a memory corruption occurring in a bit that is not used during operation, or due to the output being relatively insensitive to the parameter stored on that particular memory bit. This is thought to be an inherent effect of using (uncalibrated) mixed-signal NC hardware but could provide an SEE sensitivity that is more optimistic than is actually the case.

Fourth, in most research focused on the characterization of SEEs in devices, high-resolution oscilloscopes are used combined with precise low-dose (heavy ion) radiation equipment. Unfortunately, this was not an option as the Innatera devices have embedded circuits that do not allow direct monitoring of the electric signal. However, if specific knowledge regarding circuit design was obtainable, this might have been useful in the inspection and modeling of radiation effects.

Fifth, there are likely more radiation effects that can occur in mixed-signal neuromorphic circuits. However, these were either thought not to be detrimental to the operation of the device (e.g. displacement damage), would be very hard to distinguish based on their influence on the DUT output (e.g. differentiating between SEU and MBU), or would immediately result in a device failure (e.g. Single Event Latchup (SEL)). For all these cases, a radiation model cannot be devised in a scientifically sensible manner and were therefore left out of the scope.

The simulated T0 model has been verified against multiple prototypes to ensure relatively comparable behavior. However, these prototypes were mainly operated in a narrow range for this research. However, radiation effects might influence the NC prototype resulting in operations outside of this regime. Additional modeling would be required to assess the behavior in other operational regimes and applications. Therefore, the goal was to achieve similarity between the model and hardware in the most important regime with the most relevant parameters. This ensures that the experiments can be simulated with a large degree of similarity while the influence of non-linearities remains limited.

7.2. Future Research Directions

During the research, several choices were made to investigate areas relevant to the research questions posed in Table 3.1. To limit the scope of the project, other behavior that was not directly of interest were not explored. It is thought that these might provide valuable insight to both Innatera and the scientific community.

Firstly, the efficient operation of the NC processor is of importance for its suitability to edge processing in space applications. Also, TID effects have been demonstrated to affect the electrical performance of the used prototype. How these effects change the power consumption of the device was not explored and requires additional investigation before space applicability can be ensured.
A common effect of TID effects in electrical systems called *annealing* is related to gradual dissipation of the collected charge after irradiation. This also results in the degradation of electrical parameters to reduce slightly over time. For industrial or space applications (with fluctuating doserates), it would be interesting to see how annealing occurs in NC processors.
For hardware designers, it might be interesting to see if networks running on NC processors are more susceptible to SEUs or SETs. To investigate this, the two effects can be separated either in simulation or in experiments (by systematically overwriting parameters for each test). Addional mitigation strategies might then be applied in future NC processors to account for both effects seperately. Finally, the operational temperature of a DUT is known to influence its behavior under irradiation [85]. This is therefore an interesting correlation to investigate in order to gain more insight into how susceptible NC processors are to radiation.

7.3. Recommendations for Researchers

During this research, numerous factors came to light due to the innovative nature of the work conducted. Several guidelines concerning conventional computer architectures exist for this type of research, but new insights are proposed relating to researching the radiation sensitivity of NC hardware. These have been implemented in this research whenever possible, but due to the limited scope and available resources, they are mentioned here for future researchers.

Firstly, it is important to realize what the expected output data of the system is during experiments with respect to size and useful information. In the very early phases, the choice was made to export all raw data from the NC processor to allow for a maximum operational duty cycle during testing. This is not necessarily beneficial in all cases. Especially with respect to researching the influence of low dose rates. If one wishes to increase the exposure time, it is advised to consider lowering the duty cycle of the NC processor as well.To analyze the data, a Python library called *Polars* was employed, leveraging computational efficiency through its Rust foundation. Nonetheless, this choice constrained the exploration of alternative methods, such as spike-train analysis tools, that may have been more suitable for identifying radiation-induced disturbances.

Second, the approach used for the experiments was based on proton testing guidelines as well as simulations and discussions at Innatera. However, the full implications of testing at certain conditions were not fully understood when the testing started. This was due to the fact that an opportunistic approach was used for scheduling experiments based on beam availability. This resulted in tests being performed at imperfect conditions, failing to capture the full scope of device behavior needed for a complete analysis. Therefore, it is advised to complete the test procedure in simulation multiple times with different settings to find the full scope of interesting test conditions before physical experiments commence.

Finally, as mentioned before, the hardware used in this research is an experimental prototype. Consequently, it does not incorporate the same infrastructure that is available on production-oriented prototypes of the company. Due to the bleeding-edge nature of silicon prototypes at Innatera, the originally planned prototype was unavailable for use in this thesis project, and the planning and experiments consequently took longer to carry out. Therefore, it is advised to be aware of such potential delays depending on the exact situation and time constraints of the project.

8
Conclusions

In this chapter, the overall findings are summarized, and their significance is explained. The practical implications of this research and the potential for its application in industry are discussed. Finally, the research questions are answered.

RQ-1. How sensitive are mixed-signal neuromorphic processors to radiation?

RQ-1.1. How can Single Event Effects be modeled in mixed-signal neuromorphic processors?

In this research, it is observed that SEEs influence the processor in two ways. It can be concluded from the obtained results that parameters stored in digital memory are susceptible to SIPPs. This generally influences the nominal spiking behavior of a single NC neuron or synapse where most of the SIPPs occur in synaptic weights. Also, the firing rate of a single neuron can be momentarily influenced by SETs. This effect does not seem to have a large influence on network operation since networks generally gradually destabilize with increasing particle fluence. This indicates that SIPPs accumulating in memory result in errors in SNN operations.

RQ-1.2. How can Total Ionizing Dose be modeled in mixed-signal neuromorphic processors?

In NC processors, TID can be modeled as a homogeneous drift in neuron parameters resulting in changing spiking behavior for a given input. However, the TID effects measured in this research also have a more intricate relation to the hardware, especially the Digital-to-Analog Converter (DAC)s. Therefore, additional research is necessary to investigate what effects are hardware specific and which are generic. Overall, it is found that mixed-signal NC processors are resistant to TID. Only limited parametric degradation can be detected after heavy irradiation (200 - 800 krad(Si)), exceeding radiation levels in most LEO satellites. This indicates that mixed-signal NC processors might be suitable for space applications.

RQ-1.3. How can a model that describes SEEs in mixed-signal neuromorphic processors be validated?

The validation can be performed by operating an SNN on the NC processor that produces a predictable output if unperturbed but which is susceptible to external errors. By monitoring changes in the output, the level of radiation interaction can be retrieved. Consequently, the effects of TID, SEUs, and SETs can be isolated from each other by using a structured experimental approach where radiation exposure and device operation are toggled. The found behavior of the separate radiation effects can be used for the verification and validation of a behavioral radiation model.

RQ-1.4. How can a model of TID effects in mixed-signal neuromorphic processors be validated?

The effect of TID on a particular NC processor is difficult to validate as it is closely linked to the exact circuit characteristics and hardware. The general effect of (homogeneous) parametric degradation of the ICs might therefore translate into a non-linear deviation of initial DUT output. Unfortunately, the limited output of a NC processor complicates the investigation of potential causes for this non-linear performance degradation. Although detailed circuit information could have been beneficial, this was not accessible during the course of this research.

RQ-1.5. How does error propagation differ between mixed-signal NC processors and digital Von-Neumann architectures?

Errors are not prone to propagate in a mixed-signal NC processor due to the stochastic nature of the signals used. The amount of noise that is already present in the signal ensures that any well-trained (or tuned) SNN is not susceptible to the effects of TID or SET during operation. From the gradual destabilization of networks it can be concluded that SEU-induced errors can accumulate leading to destabilization of network operation and architecture disruption which results in failure over time.

RQ-2. How can radiation effects on mixed-signal neuromorphic processors and their effect on SNN operation be mitigated?

RQ-2.1. How can fault tolerance be implemented on SNNs?

From the results in section 6.2, it is clear that measures can be applied to increase the fault tolerance of existing SNNs. Changing network parameters such as increasing the group size by adding redundant neurons or synapses is effective. Small changes with respect to these parameters can already increase the fault tolerance of a synfire chain with a factor of 2x-3x. Also, conventional techniques used in many space applications such as TMR and frequently re-initializing parameters (or resetting the system) can significantly increase fault tolerance. These mitigation methods can be applied in NC, albeit at the cost of degrading operational performance and increasing memory and the necessary number of neurons and synapses on the chip.

RQ-2.2 How can strategies for mitigating radiation-induced errors in mixed-signal neuromorphic processors be validated?

Validating if a particular mitigation strategy correctly improves the fault tolerance of a network is a difficult task. In this research, a basic approach was used by employing a standard synfire chain and adding mitigation measures to it in varying degrees. By injecting these SNNs with perturbations modeled after experimental radiation effects, the network operation is found to destabilize at different instances. The most important indicator of destabilization for a synfire chain is the cycle duration t_c and the causality c. If the number of injected perturbations is compared across different strategies, a sense of the efficiency of radiation effect mitigation can be found. Through a comparison between these numbers and experimentally observed data (concerning redundant neurons and increased synaptic weights) it is possible to validate whether the mitigation strategies enhance fault-tolerance. However, simulated mitigation methods that were not implementable in hardware could not be appropriately validated.

Bibliography

[1] UCS. *Satellite Database | Union of Concerned Scientists*. May 2022.
url: https://www.ucsusa.org/resources/satellite-database.

[2] Alessandro De Concini and Jaroslav Toth. *The future of the European space sector*. Tech. rep. European Investment Bank, 2020.

[3] Martin N. Sweeting. “Modern Small Satellites - Changing the Economics of Space”. In: *Proceedings of the IEEE* 106.3 (Mar. 2018), pp. 343–361. issn: 0018-9219. doi: 10.1109/JPROC.2018.2806218. url: https://openresearch.surrey.ac.uk/esploro/outputs/journalArticle/Modern-Small-Satellites---Changing-the-Economics-of-Space/99512072802346.

[4] Daniel Selva and David Krejci.
“A survey and assessment of the capabilities of Cubesats for Earth observation”.
In: *Acta Astronautica* 74 (May 2012), pp. 50–68. issn: 0094-5765.
doi: 10.1016/j.actaastro.2011.12.014.
url: www.elsevier.com/locate/actaastro.

[5] Weisong Shi et al. “Edge Computing: Vision and Challenges”.
In: *IEEE Internet of Things Journal* 3.5 (Oct. 2016), pp. 637–646. issn: 23274662.
doi: 10.1109/JIOT.2016.2579198.

[6] Gianluca Giuffrida et al.
“CloudScout: A Deep Neural Network for On-Board Cloud Detection on Hyperspectral Images”.
In: *Remote Sensing* 12.14 (July 2020), p. 2205. issn: 2072-4292. doi: 10.3390/RS12142205.
url: https://www.mdpi.com/2072-4292/12/14/2205/htm%20https://www.mdpi.com/2072-4292/12/14/2205.

[7] Jason Swope et al.
“BENCHMARKING REMOTE SENSING IMAGE PROCESSING AND ANALYSIS ON THE SNAPDRAGON PROCESSOR ONBOARD THE INTERNATIONAL SPACE STATION”.
In: *2022 IEEE International Geoscience and Remote Sensing Symposium*. 2022.

[8] Bradley Denby and Brandon Lucia.
“Orbital edge computing: Nanosatellite constellations as a new class of computer system”.
In: *International Conference on Architectural Support for Programming Languages and Operating Systems - ASPLOS* (Mar. 2020), pp. 939–954. doi: 10.1145/3373376.3378473.
url: https://doi.org/10.1145/3373376.3378473.

[9] Emily Dunkel et al. “BENCHMARKING DEEP LEARNING INFERENCE OF REMOTE SENSING IMAGERY ON THE QUALCOMM SNAPDRAGON AND INTEL MOVIDIUS MYRIAD X PROCESSORS ONBOARD THE INTERNATIONAL SPACE STATION”.
In: *2022 IEEE International Geoscience and Remote Sensing Symposium*. 2022.

[10] Vasco Medici et al. *Neuromorphic computation of optic flow data Bio-inspired landing using biomorphic vision sensors Final Report*. Tech. rep. European Space Agency, 2010.
url: http://www.esa.int/act.

[11] J. L. Taggart et al.
“In Situ Synaptic Programming of CBRAM in an Ionizing Radiation Environment”.
In: *IEEE Transactions on Nuclear Science* 65.1 (Jan. 2018), pp. 192–199. issn: 00189499.
doi: 10.1109/TNS.2017.2779860.

[12] Rong Jiang et al. “Total-Ionizing-Dose Response of Nb2O5-Based MIM Diodes for Neuromorphic Computing Applications”.
In: *IEEE Transactions on Nuclear Science* 65.1 (Jan. 2018), pp. 78–83. issn: 00189499.
doi: 10.1109/TNS.2017.2761904.

[13] Vinod K. Sangwan and Mark C. Hersam. "Neuromorphic nanoelectronic materials". In: *Nature Nanotechnology 2020 15:7* 15.7 (Mar. 2020), pp. 517–528. issn: 1748-3395. doi: `10.1038/S41565-020-0647-Z`. url: `https://www-nature-com.tudelft.idm.oclc.org/articles/s41565-020-0647-z`.

[14] R. Ecoffet. "Overview of in-orbit radiation induced spacecraft anomalies". In: *IEEE Transactions on Nuclear Science* 60.3 (2013), pp. 1791–1815. issn: 00189499. doi: `10.1109/TNS.2013.2262002`.

[15] Edward Petersen. *Single Event Effects in Aerospace*. WILEY, 2011. isbn: 9781118084328. url: `https://ieeexplore-ieee-org.tudelft.idm.oclc.org/xpl/ebooks/bookPdfWithBanner.jsp?fileName=6047596.pdf&bkn=6047596&pdfType=book`.

[16] Gennadi Bersuker, Maribeth Mason, and Karen L Jones. "NEUROMORPHIC COMPUTING: THE POTENTIAL FOR HIGH-PERFORMANCE PROCESSING IN SPACE". In: *AEROSPACE* (2018), pp. 1–12.

[17] Dario Izzo et al. "Neuromorphic Computing and Sensing in Space". In: (Dec. 2022). url: `https://arxiv.org/abs/2212.05236v2`.

[18] Justin Goodwill et al. "NASA SpaceCube Edge TPU SmallSat Card for Autonomous Operations and Onboard Science-Data Analysis". In: *Proceedings of the Small Satellite Conference*. AIAA, 2021.

[19] Qualcomm. *Journey to Mars: How our collaboration with Jet Propulsion Laboratory fostered innovation*. 2021. url: `https://www.qualcomm.com/news/onq/2021/03/journey-mars-how-our-collaboration-jet-propulsion-laboratory-fostered-innovation`.

[20] NASA. *Deep Neural Net and Neuromorphic Processors for In-Space Autonomy and Cognition*. Tech. rep. NASA, 2019. url: `https://arxiv.org/pdf/1705.06963`.

[21] Pablo Miralles et al. "A critical review on the state-of-the-art and future prospects of machine learning for Earth observation operations". In: (). doi: `10.1016/j.asr.2023.02.025`. url: `www.elsevier.com/locate/asrAvailableonlineatwww.sciencedirect.com`.

[22] Seth Roffe et al. "Neutron-Induced, Single-Event Effects on Neuromorphic Event-Based Vision Sensor: A First Step and Tools to Space Applications". In: *IEEE Access* 9 (2021), pp. 85748–85763. issn: 21693536. doi: `10.1109/ACCESS.2021.3085136`.

[23] Tao Sun, Bojian Yin, and Sander Bohte. "Efficient Uncertainty Estimation in Spiking Neural Networks via MC-dropout". In: (Apr. 2023). url: `https://arxiv.org/abs/2304.10191v1`.

[24] Michael Hopkins et al. "Spiking neural networks for computer vision". In: *Interface Focus* 8.4 (Aug. 2018). issn: 20428901.

[25] Wulfram Gerstner and Werner Kistler. *Spiking Neuron Models*. 1st ed. Cambridge University Press, 2002. isbn: 9780511076602.

[26] Maxence Bouvier et al. "Spiking Neural Networks Hardware Implementations and Challenges". In: *ACM Journal on Emerging Technologies in Computing Systems (JETC)* 15.2 (Apr. 2019). issn: 15504840. doi: `10.1145/3304103`. url: `https://dl-acm-org.tudelft.idm.oclc.org/doi/abs/10.1145/3304103`.

[27] Andrzej S. Kucik and Gabriele Meoni. *Investigating Spiking Neural Networks for Energy-Efficient On-Board AI Applications. A Case Study in Land Cover and Land Use Classification*. 2021.

[28] Bing Han et al. "Cross-Layer Design Exploration for Energy-Quality Tradeoffs in Spiking and Non-Spiking Deep Artificial Neural Networks". In: *IEEE Transactions on Multi-Scale Computing Systems* 4.4 (Oct. 2018), pp. 613–623. issn: 23327766. doi: `10.1109/TMSCS.2017.2737625`.

[29] K. Moon et al. “RRAM-based synapse devices for neuromorphic systems”. In: *Faraday Discussions* 213.0 (Feb. 2019), pp. 421–451. issn: 1364-5498. doi: 10.1039/C8FD00127H. url: https://pubs-rsc-org.tudelft.idm.oclc.org/en/content/articlehtml/2019/fd/c8fd00127h%20https://pubs-rsc-org.tudelft.idm.oclc.org/en/content/articlelanding/2019/fd/c8fd00127h.

[30] Carver Mead and Mohammed Ismail. *Analog VLSI Implementation of Neural Systems*. Vol. 80. Springer Science & Business Media, 1989. url: https://books.google.nl/books?hl=en&lr=&id=9e29dOiXeiMC&oi=fnd&pg=PP13&dq=Analog+VLSI+implementation+of+neural+systems&ots=cf-j4rUvVJ&sig=-Mkg799t19CxWe7wMUUkjB1lskI&redir_esc=y#v=onepage&q=Analog%20VLSI%20implementation%20of%20neural%20systems&f=false.

[31] Steve Furber. “Large-scale neuromorphic computing systems”. In: *Journal of Neural Engineering* 13.5 (Aug. 2016). issn: 17412552. doi: 10.1088/1741-2560/13/5/051001.

[32] Peter Sterling and Simon Laughlin. *Principles of Neural Design*. Cambridge: MIT Press, 2015.

[33] Romain Brette and Wulfram Gerstner. “Adaptive exponential integrate-and-fire model as an effective description of neuronal activity”. In: *Journal of Neurophysiology* 94.5 (Nov. 2005), pp. 3637–3642. issn: 00223077. doi: 10.1152/JN.00686.2005/ASSET/IMAGES/LARGE/Z9K0110549990003.JPEG. url: https://journals.physiology.org/doi/10.1152/jn.00686.2005.

[34] Eugene M. Izhikevich. “Simple model of spiking neurons”. In: *IEEE Transactions on Neural Networks* 14.6 (Nov. 2003), pp. 1569–1572. issn: 10459227. doi: 10.1109/TNN.2003.820440.

[35] Catherine D. Schuman et al. “A Survey of Neuromorphic Computing and Neural Networks in Hardware”. In: *arXiv* (May 2017). doi: 10.48550/arxiv.1705.06963. url: https://arxiv.org/abs/1705.06963v1.

[36] Rick Alena. “Radiation and Fault Tolerance for Neuromorphic Computing”. In: ().

[37] *NEUROMORPHIC COMPUTING FOR SPACE – Air Force Research Laboratory*. url: https://afresearchlab.com/technology/nics.

[38] Yulia Sandamirskaya et al. “Neuromorphic computing hardware and neural architectures for robotics”. In: *Science Robotics* 7.67 (June 2022), p. 8419. issn: 2470-9476. doi: 10.1126/SCIROBOTICS.ABL8419. url: https://www-science-org.tudelft.idm.oclc.org/doi/10.1126/scirobotics.abl8419.

[39] Ning Qiao et al. “A reconfigurable on-line learning spiking neuromorphic processor comprising 256 neurons and 128K synapses”. In: *Frontiers in Neuroscience* 9.APR (2015), p. 141. issn: 1662453X. doi: 10.3389/FNINS.2015.00141/ABSTRACT.

[40] Saber Moradi et al. “A Scalable Multicore Architecture with Heterogeneous Memory Structures for Dynamic Neuromorphic Asynchronous Processors (DYNAPs)”. In: *IEEE Transactions on Biomedical Circuits and Systems* 12.1 (Feb. 2018), pp. 106–122. issn: 19324545. doi: 10.1109/TBCAS.2017.2759700.

[41] Markus Levy. *INNATERA’S SPIKING NEURAL PROCESSOR Brain-Like Architecture Targets Ultra-Low-Power AI*. Tech. rep. The Linley Group, 2021. url: www.linleygroup.com/.

[42] Johannes Schemmel et al. “A wafer-scale neuromorphic hardware system for large-scale neural modeling”. In: *ISCAS 2010 - 2010 IEEE International Symposium on Circuits and Systems: Nano-Bio Circuit Fabrics and Systems* (2010), pp. 1947–1950. doi: 10.1109/ISCAS.2010.5536970.

[43] Yannik Stradmann et al. “Demonstrating Analog Inference on the BrainScaleS-2 Mobile System”. In: (Mar. 2021). doi: 10.48550/arxiv.2103.15960. url: https://arxiv.org/abs/2103.15960v2.

[44] Andreas Grübl et al. "Verification and Design Methods for the BrainScaleS Neuromorphic Hardware System". In: *Journal of Signal Processing Systems* 92.11 (Nov. 2020), pp. 1277–1292. issn: 19398115. doi: 10.1007/S11265-020-01558-7/FIGURES/11. url: https://link-springer-com.tudelft.idm.oclc.org/article/10.1007/s11265-020-01558-7.

[45] Paul A. Merolla et al. "A million spiking-neuron integrated circuit with a scalable communication network and interface". In: *Science* 345.6197 (Aug. 2014), pp. 668–673. issn: 10959203. doi: 10.1126/SCIENCE.1254642/SUPPL{_}FILE/MEROLLA.SM.REV1.PDF. url: https://www-science-org.tudelft.idm.oclc.org/doi/10.1126/science.1254642.

[46] Steve B. Furber et al. "The SpiNNaker project". In: *Proceedings of the IEEE* 102.5 (2014), pp. 652–665. issn: 00189219. doi: 10.1109/JPROC.2014.2304638.

[47] Mike Davies et al. "Loihi: A Neuromorphic Manycore Processor with On-Chip Learning". In: *IEEE Micro* 38.1 (Jan. 2018), pp. 82–99. issn: 02721732. doi: 10.1109/MM.2018.112130359.

[48] Jing Pei et al. "Towards artificial general intelligence with hybrid Tianjic chip architecture". In: *Nature* 572.7767 (July 2019), pp. 106–111. issn: 1476-4687. doi: 10.1038/S41586-019-1424-8. url: https://www-nature-com.tudelft.idm.oclc.org/articles/s41586-019-1424-8.

[49] E. G. Stassinopoulos and James P. Raymond. "The Space Radiation Environment for Electronics". In: *Proceedings of the IEEE* 76.11 (1988), pp. 1423–1442. issn: 15582256. doi: 10.1109/5.90113.

[50] E. R. Benton and E. V. Benton. "Space radiation dosimetry in low-Earth orbit and beyond". In: *Nuclear Instruments and Methods in Physics Research Section B: Beam Interactions with Materials and Atoms* 184.1-2 (Sept. 2001), pp. 255–294. issn: 0168-583X. doi: 10.1016/S0168-583X(01)00748-0.

[51] Sophie Duzellier. "Radiation effects on electronic devices in space". In: *Aerospace Science and Technology* 9.1 (Jan. 2005), pp. 93–99. issn: 1270-9638. doi: 10.1016/J.AST.2004.08.006.

[52] Tony C Slaba, Steve R Blattnig, and John W Norbury. *Space Radiation Environment Comparison and Validation of GCR Models Briefing to NAC HEO/SMD Joint Committee April 2015*.

[53] NASA. *NASA: Van Allen Belts*. Sept. 2022. url: https://image.gsfc.nasa.gov/poetry/tour/AAvan.html.

[54] Hervé Cottin et al. "Space as a Tool for Astrobiology: Review and Recommendations for Experimentations in Earth Orbit and Beyond". In: *Space Science Reviews 2017 209:1* 209.1 (June 2017), pp. 83–181. issn: 1572-9672. doi: 10.1007/S11214-017-0365-5. url: https://link-springer-com.tudelft.idm.oclc.org/article/10.1007/s11214-017-0365-5.

[55] Patrick M. O'Neill. "Badhwar-O'Neill 2010 galactic cosmic ray flux model - Revised". In: *IEEE Transactions on Nuclear Science* 57.6 PART 1 (Dec. 2010), pp. 3148–3153. issn: 00189499. doi: 10.1109/TNS.2010.2083688.

[56] R. A. Nymmik, M. I. Panasyuk, and A. A. Suslov. "Galactic cosmic ray flux simulation and prediction". In: *Advances in Space Research* 17.2 (Jan. 1996), pp. 19–30. issn: 0273-1177. doi: 10.1016/0273-1177(95)00508-C.

[57] Paul R. Boberg et al. "CREME96: A revision of the cosmic ray effects on micro-electronics code". In: *IEEE Transactions on Nuclear Science* 44.6 PART 1 (1997), pp. 2150–2160. issn: 00189499. doi: 10.1109/23.659030.

[58] G P Ginet et al. “Space Sci Rev AE9, AP9 and SPM: New Models for Specifying the Trapped Energetic Particle and Space Plasma Environment”. In: *Space Scientific Review* (2013). doi: 10.1007/s11214-013-9964-y.

[59] W Robert Johnston et al. “AE9/AP9/SPM: New Models for Radiation Belt and Space Plasma Specification”. In: (2014). doi: 10.1117/12.2049836. url: http://spiedl.org/terms.

[60] Yifan Lu et al. “A Review of the Space Environment Effects on Spacecraft in Different Orbits”. In: *IEEE Access* 7 (2019), pp. 93473–93488. issn: 21693536. doi: 10.1109/ACCESS.2019.2927811.

[61] Kurt Anderson. “Low-cost, radiation-tolerant, on-board processing solution”. In: *IEEE Aerospace Conference Proceedings* 2005 (2005). issn: 1095323X. doi: 10.1109/AERO.2005.1559533.

[62] Robert Baumann. “Soft errors in advanced computer systems”. In: *IEEE Design and Test of Computers* 22.3 (May 2005), pp. 258–266. issn: 07407475. doi: 10.1109/MDT.2005.69.

[63] Wenzhe Guo et al. “Neural Coding in Spiking Neural Networks: A Comparative Study for Robust Neuromorphic Systems”. In: *Frontiers in Neuroscience* 15 (Mar. 2021). issn: 1662453X. doi: 10.3389/FNINS.2021.638474.

[64] Chankyu Lee et al. “Enabling Spike-Based Backpropagation for Training Deep Neural Network Architectures”. In: *Frontiers in Neuroscience* 14 (Feb. 2020). issn: 1662453X. doi: 10.3389/FNINS.2020.00119.

[65] A. L. Hodgkin and A. F. Huxley. “A quantitative description of membrane current and its application to conduction and excitation in nerve”. In: *Bulletin of Mathematical Biology 1990 52:1* 52.1 (Jan. 1990), pp. 25–71. issn: 1522-9602. doi: 10.1007/BF02459568. url: https://link.springer.com/article/10.1007/BF02459568.

[66] Warren S. McCulloch and Walter Pitts. “A logical calculus of the ideas immanent in nervous activity”. In: *The bulletin of mathematical biophysics 1943 5:4* 5.4 (Dec. 1943), pp. 115–133. issn: 1522-9602. doi: 10.1007/BF02478259. url: https://link.springer.com/article/10.1007/BF02478259.

[67] Fopefolu Folowosele, Ralph Etienne-Cummings, and Tara Julia Hamilton. “A CMOS switched capacitor implementation of the Mihalas-Niebur neuron”. In: *2009 IEEE Biomedical Circuits and Systems Conference, BioCAS 2009* (2009), pp. 105–108. doi: 10.1109/BIOCAS.2009.5372072.

[68] Paolo Livi and Giacomo Indiveri. “A current-mode conductance-based silicon neuron for Address-Event neuromorphic systems”. In: *Proceedings - IEEE International Symposium on Circuits and Systems* (2009), pp. 2898–2901. issn: 02714310. doi: 10.1109/ISCAS.2009.5118408.

[69] Shih-Chii Liu, Jörg Kramer, and Giacomo Indiveri. *Analog VLSI: Circuits and Principles*. MIT Press, 2002. url: https://ieeexplore-ieee-org.tudelft.idm.oclc.org/book/6267299.

[70] Stefano Fusi and L. F. Abbott. “Limits on the memory storage capacity of bounded synapses”. In: *Nature Neuroscience 2007 10:4* 10.4 (Mar. 2007), pp. 485–493. issn: 1546-1726. doi: 10.1038/nn1859. url: https://www.nature.com/articles/nn1859.

[71] Daniel J. Amit and Stefano Fusi. “Constraints on learning in dynamic synapses”. In: *Network: Computation in Neural Systems* 3.4 (1992), pp. 443–464. issn: 0954898X. doi: 10.1088/0954-898X{_}3{_}4{_}008. url: https://www.tandfonline.com/doi/abs/10.1088/0954-898X_3_4_008.

[72] ECSS. *Space engineering Methods for the calculation of radiation received and its effects, and a policy for design margins*. Tech. rep. ECSS, 2008.

[73] T. R. Oldham and F. B. McLean. “Total ionizing dose effects in MOS oxides and devices”. In: *IEEE Transactions on Nuclear Science* 50 III.3 (June 2003), pp. 483–499. issn: 00189499. doi: 10.1109/TNS.2003.812927.

[74] ECSS-E-HB-10-12A. *Space engineering: Calculation of radiation and its effects and margin policy handbook*. 2010.

[75] Dan F. M. Goodman and Romain Brette. *Brian simulator*. 2013. doi: 10.4249/SCHOLARPEDIA.10883.

[76] Nicholas T. Carnevale and Michael L. Hines. *The NEURON Book*. Cambridge University Press, 2006. url: https://books.google.nl/books?hl=en&lr=&id=YzcOyjKBPHgC&oi=fnd&pg=PA1&ots=Km8IGr2ZJf&sig=CADR9S66OHiEZN1NSCx2r68frLA&redir_esc=y#v=onepage&q&f=false.

[77] Marc-Oliver Gewaltig and Markus Diesmann. *NEST (NEural Simulation Tool)*. 2007. doi: 10.4249/SCHOLARPEDIA.1430.

[78] Marcel Stimberg, Romain Brette, and Dan F.M. Goodman. “Brian 2, an intuitive and efficient neural simulator”. In: *eLife* 8 (Aug. 2019). issn: 2050084X. doi: 10.7554/ELIFE.47314.

[79] Henry C. Tuckwell. *Stochastic Processes in the Neurosciences*. Society for Industrial and Applied Mathematics, Jan. 1989. isbn: 978-0-89871-232-2. doi: 10.1137/1.9781611970159. url: http://epubs.siam.org/doi/book/10.1137/1.9781611970159.

[80] Moshe Abeles. *Corticonics: Neural Circuits of the Cerebral Cortex*. Cambridge University Press, 1991, pp. 227–258. isbn: 0-521-37476-6.

[81] Marc-Oliver Gewaltig, Markus Diesmann, and Ad Aertsen. “Propagation of cortical synfire activity: survival probability in single trials and stability in the mean”. In: *Neural networks* 14.6 (2001), pp. 657–673. url: www.elsevier.com/locate/neunet.

[82] Markus Diesmann, Marc Oliver Gewaltig, and Ad Aertsen. “Stable propagation of synchronous spiking in cortical neural networks”. In: *Nature 1999 402:6761* 402.6761 (Dec. 1999), pp. 529–533. issn: 1476-4687. doi: 10.1038/990101. url: https://www-nature-com.tudelft.idm.oclc.org/articles/990101.

[83] Y. Boulghassoul et al. “Frequency domain analysis of analog single-event transients in linear circuits”. In: *IEEE Transactions on Nuclear Science* 49 I.6 (Dec. 2002), pp. 3142–3147. issn: 00189499. doi: 10.1109/TNS.2002.805330.

[84] Stephen Buchner et al. *Proton Test Guideline Development-Lessons Learned For: NASA Electronic Parts and Packaging (NEPP) Program Electronics Radiation Characterization (ERC) Project And Defense Threat Reduction Agency*. Tech. rep. NASA, 2002.

[85] “JEDEC STANDARD TEST STANDARD FOR THE MEASUREMENT OF PROTON RADIATION SINGLE EVENT EFFECTS IN ELECTRONIC DEVICES JESD234 OCTOBER 2013 JEDEC SOLID STATE TECHNOLOGY ASSOCIATION”. In: (). url: www.jedec.org.

[86] M Rovituso et al. “Characterisation of the HollandPTC R&D proton beamline for physics and radiobiology studies”. In: ().

[87] Angélica Pérez-Andújar et al. “The physics of proton therapy ”. In: *Physics in Medicine & Biology TOPICAL REVIEW • OPEN ACCESS* 60 (2015), p. 155. doi: 10.1088/0031-9155/60/8/R155.

[88] James F Ziegler, M D Ziegler, and J P Biersack. “SRIM – The stopping and range of ions in matter (2010)”. In: (2010). doi: 10.1016/j.nimb.2010.02.091. url: www.SRIM.org..

[89] B. N. Tejas, Kakumani Shanmuka Kumar, and S. M. Sunita. “Multiple Bit Error Correction Codes for Memories in Satellites”. In: *2022 IEEE 7th International conference for Convergence in Technology (I2CT)* (2022). doi: 10.1109/I2CT54291.2022.9824813.

[90] Michael J Campola and Jonathan A Pellish. *Radiation Hardness Assurance: Evolving for NewSpace NASA Electronic Parts Manager / NASA Electronic Parts and Packaging (NEPP) Program Deputy Manager*. 2019.

[91] Leonie Buckley et al. “Radiation Test and in Orbit Performance of MpSoC AI Accelerator”. In: *2022 IEEE Aerospace Conference (AERO)* (Mar. 2022), pp. 1–9. doi: 10.1109/AERO53065.2022.9843440. url: https://ieeexplore.ieee.org/document/9843440/.

[92] Megan Casey, Ed Wyrwas, and Rebekah Austin. *Recent Radiation Test Results on COTS AI Edge Processing ASICs*. 2022.

[93] S. W. Samwel and A. A. Hady. “Space radiation environment forecast for EGYPTSAT-2 satellite”. In: *Space Weather* 7.12 (Dec. 2009). issn: 1542-7390. doi: 10.1029/2009SW000482. url: https://onlinelibrary-wiley-com.tudelft.idm.oclc.org/doi/full/10.1029/2009SW000482%20https://onlinelibrary-wiley-com.tudelft.idm.oclc.org/doi/abs/10.1029/2009SW000482%20https://agupubs-onlinelibrary-wiley-com.tudelft.idm.oclc.org/doi/10.1029/2009SW000482.

[94] M. A. Xapsos et al. “Model for solar proton risk assessment”. In: *IEEE Transactions on Nuclear Science* 51.6 II (Dec. 2004), pp. 3394–3398. issn: 00189499. doi: 10.1109/TNS.2004.839159. url: https://www.researchgate.net/publication/3139146_Model_for_solar_proton_risk_assessment.